Condensin I^{DC}, H4K20me1, and perinuclear tethering maintain X chromosome repression in *C. elegans*

Jessica Trombley, Audry I. Rakozy, Eshna Jash, Györgyi Csankovszki*

Department of Molecular, Cellular, and Developmental Biology, University of Michigan, Ann Arbor, Michigan, United States of America

*corresponding author

e-mail: gyorgyi@umich.edu

Abstract

Dosage compensation in *Caenorhabditis elegans* equalizes X-linked gene expression between XX hermaphrodites and XO males. The process depends on a condensin-containing dosage compensation complex (DCC), which binds the X chromosomes in hermaphrodites to repress gene expression. Condensin I^{DC} and an additional five DCC components must be present on the X during early embryogenesis in hermaphrodites to establish dosage compensation. However, whether the DCC's continued presence is required to maintain the repressed state once established is unknown. Beyond the role of condensin I^{DC} in X chromosome compaction, additional mechanisms contribute to X-linked gene repression. DPY-21, a non-condensin I^{DC} DCC component, is an H4K20me2/3 demethylase whose activity enriches the repressive histone mark, H4 lysine 20 monomethylation, on the X chromosomes. In addition, CEC-4 tethers H3K9me3-rich chromosomal regions to the nuclear lamina, which also contributes to X-linked gene repression. To investigate the necessity of condensin I^{DC} during the larval and adult stages of hermaphrodites, we used the auxin-inducible degradation system to deplete the condensin I^{DC} subunit DPY-27. While DPY-27 depletion in the embryonic stages resulted in lethality, DPY-27 depleted larvae and adults survive. In these DPY-27 depleted strains, condensin I^{DC} was no longer associated with the X chromosome, the X became decondensed, and the H4K20me1 mark was gradually lost, leading to X-linked gene derepression. These results suggest that the stable maintenance of dosage compensation requires the continued presence of condensin I^{DC}. A loss-of-function mutation in *cec-4*, in addition to the depletion of DPY-27 or the genetic mutation of *dpy-21*, led to even more significant increases in X-linked gene expression, suggesting that tethering heterochromatic regions to the nuclear lamina helps stabilize repression mediated by condensin I^{DC} and H4K20me1.

Author Summary

In some organisms, whether an individual becomes male, female, or hermaphrodite is determined by the number of their sex chromosomes. In the nematode *Caenorhabditis elegans*, males have one X chromosome, whereas hermaphrodites have two X chromosomes. This difference in the number of X chromosomes is crucial for deciding whether an individual becomes a hermaphrodite or a male. However, having two X chromosomes can lead to problems because it results in different gene expression levels, resulting in hermaphrodite lethality. To solve this issue, many organisms undergo a process called dosage compensation. Dosage compensation in *C. elegans* is achieved by a group of proteins known as the dosage compensation complex (DCC), which includes a protein called DPY-27. The function of DPY-27 is essential during early embryonic development. This study shows that in contrast to early embryonic development, larvae and adults can still survive when DPY-27 is missing. In these worms, all known mechanisms involved in dosage compensation are disrupted and the X is no longer repressed. Our results suggest that the maintenance of dosage compensation in nematodes is an active process, and that it is essential for survival

when the organism is developing, but once fully developed, the process becomes dispensable.

Introduction

Chromosome conformation, subnuclear localization, and the post-translational modifications of histones are closely linked to gene expression. The relationship between these processes plays a crucial role in an organism's development, growth, and survival. Dosage compensation in the nematode *Caenorhabditis elegans* offers an excellent paradigm for exploring chromosome-wide gene regulation.

There is an inherent imbalance in chromosomal gene expression in species with heterogametic sexes [1]. As in numerous other species with chromosome-based sex determination, *C. elegans* has evolved several molecular mechanisms to ensure equal gene expression from the sex chromosomes between the sexes [2]. This process is known as dosage compensation. In *C. elegans,* hermaphrodites have two X chromosomes (2X:2A), whereas males have only one X and no other sex chromosome (1X:2A) [3]. This difference in chromosome count is essential for sex determination [3,4]. However, without correction, in hermaphrodites, transcription from the X doubles relative to males, leaving the hermaphrodite population inviable [5]. The dosage compensation mechanism in *C. elegans* corrects for the differing numbers of sex chromosomes by reducing the gene expression of the hermaphrodite X chromosomes [6]. Dosage compensation requires orchestrating several gene-regulatory events across X chromosomes in hermaphrodites to decrease gene expression by half.

A core component of the dosage compensation machinery in *C. elegans* involves a specialized condensin complex. Condensins are highly conserved protein complexes used in most cellular life, from prokaryotes to metazoans [7]. Condensin complexes are characterized by their ring-shaped structure, and they hydrolyze ATP to extrude DNA strands through the ring, thus leading to DNA coiling and loop formation [8]. This loop extrusion activity is thought to be essential for chromosome compaction in mitosis and meiosis [9]. Multicellular eukaryotes have two condensin complexes, condensin I and II, functioning in mitosis and meiosis [10]. Similarly, *C. elegans* utilizes condensin I and II complexes for chromosome compaction and segregation [11]. However, *C. elegans* has a third condensin complex that specifically functions in dosage compensation of the X chromosomes of hermaphrodites. The hermaphrodite-specific condensin is known as condensin I^{DC} (Dosage Compensation) [11,12]. Condensins are composed of two structural maintenance of chromosomes (SMC) proteins and three chromosome-associated polypeptides (CAP) [13,14]. Condensin I^{DC} earns its name due to the four shared protein subunits with condensin I. These subunits include the structural maintenance of chromosomes (SMC) protein MIX-1 and the chromosome-associated polypeptides (CAPs) CAPG-1, DPY-26, and DPY-28. The difference between condensin I^{DC} and condensin I is the second SMC subunit, DPY-27 in condensin I^{DC} and its paralog SMC-4 in condensin I [11,15,16]. Condensin I^{DC} compacts the dosage compensated X chromosomes; thus, the X occupies less nuclear volume in

hermaphrodites than in males [17,18]. At a higher resolution, condensin I^{DC} remodels the architecture of the X chromosomes to form topologically associating domains (TADs) characterized by a higher frequency of *cis*-interactions within domains [19,20].

Beyond condensin I^{DC}, the complete dosage compensation complex (DCC) in *C. elegans* includes the proteins SDC-1, SDC-2, SDC-3, DPY-30, and DPY-21 [11,21–23]. Together, these ten proteins bind and spread across the X chromosomes in hermaphrodites, inhibiting RNA Pol II binding, thus lowering transcriptional output by half [24]. One of the non-condensin DCC subunits is DPY-21 [22]. It contains a Jumonji C domain found in histone demethylases. DPY-21 has been shown to demethylate dimethylated histone 4 lysine 20 (H4K20me2) [25], previously deposited on histones by the activities of SET-1 and SET-4 [26,27], to the monomethylated form (H4K20me1). Thus, by the X-specific demethylase activity of DPY-21, H4K20me1 is enriched on the X chromosomes in hermaphrodites and contributes to further repression [25–27]. In addition to its demethylase function, DPY-21 has an additional uncharacterized role in dosage compensation [25,28]. Like other DCC members, DPY-21 activity is required to regulate the X chromosome effectively, as evidenced by the elevated X-linked gene expression in hermaphrodites with *dpy-21* mutations [25,29]. However, DPY-21 is not necessary to recruit the other DCC members, and the loss of its function leads to mild defects in hermaphrodite *C. elegans* but no significant lethality [22].

Nuclear lamina interactions with heterochromatin provide an additional layer of gene regulation in *C. elegans,* impacting dosage compensation. In *C. elegans,* heterochromatic regions of chromosomes are located near the nuclear periphery [29,30]. Histone methyl transferases (HMTs) MET-2 and SET-25 target H3 lysine 9 (H3K9) on chromatin to deposit mono-, di-, and trimethylation [30]. The lamina-associated protein CEC-4 binds to heterochromatic H3K9me regions on both the autosomes and the X [32]. The tethering of heterochromatic regions of the chromosomes to the nuclear lamina contributes to stabilizing cell fates during *C. elegans* development [32]. In addition, the loss of nuclear lamina tethering leads to the decompaction and relocation of the X into a more interior position in the nucleus and a mild increase of X-linked gene expression without impacting autosomal gene expression, indicating dosage compensation defects [33]. Despite defects in the chromosomal organization, mutants with non-functional CEC-4 survive with no apparent phenotypes [32].

Dosage compensation is set up in a stepwise manner over the course of development in *C. elegans*. The process is initiated around the 40-cell stage, when the DCC subunit SDC-2 is expressed and localizes to hermaphrodite X chromosomes [34], which leads to the recruitment of the other DCC subunits [35]. This initiation step coincides with the loss of pluripotency of embryonic blastomeres [36,37]. DPY-21 localizes to the X after the initial loading of condensin I^{DC}, and H4K20me1 becomes enriched on the X between the bean and comma stages of embryogenesis [25,36]. By the end of embryogenesis, most cells exit mitosis [38], after which the dosage-compensated state is maintained in

postmitotic cells. We refer to this stage as the maintenance phase. Earlier studies using cold-sensitive *dpy-27* alleles suggested that DPY-27 activity is essential during a critical developmental time window in mid-embryogenesis, after which loss of its function has a lesser impact on viability [39]. These results suggest that while condensin I^{DC} is required to initiate dosage compensation, other mechanisms may be responsible for maintaining dosage compensation, including ones mediated by DPY-21 and CEC-4.

The requirement for CEC-4 also changes with the differentiation state of embryonic cells. CEC-4 is required to tether heterochromatic transgenic arrays to the nuclear lamina in embryos but not in L1 larvae [32]. At the larval stages and beyond, additional mechanisms, including ones mediated by MRG-1 and CBP-1, contribute to sequestering heterochromatin to the nuclear lamina [40]. However, X chromosome compaction and nuclear lamina tethering are affected in *cec-4* adults, even in fully differentiated postmitotic cells [33]. We hypothesize that by sequestering the chromosome to the nuclear lamina, CEC-4 stabilizes the repression of the X chromosomes during the maintenance phase of dosage compensation.

In this study, we used the auxin-inducible degradation (AID) system to deplete the condensin I^{DC} subunit DPY-27 at various stages of development. We assessed the importance of condensin I^{DC} to X chromosome repression and organismal viability during the establishment and maintenance phases of dosage compensation. Our findings reveal that the continued presence of DPY-27 is required to maintain X chromosome repression after initial establishment. However, continued repression is less essential for viability during the maintenance phase. Additionally, we evaluated the hypothesis that the nuclear lamina protein CEC-4 helps stabilize the repressed state by combining *cec-4* mutations with depletion of DPY-27 or mutations in the histone demethylase *dpy-21.* We show that the loss of lamina associations resulting from mutations in *cec-4* exacerbates the defects caused by the lack of DPY-27 or DPY-21 function. Our results reveal the differential contributions of the various repressive pathways to X chromosome dosage compensation.

Results

The impact of DPY-27 depletion on hermaphrodite embryos and larvae

Using a strain containing an auxin-inducible degron (AID)-tagged *dpy-27* allele [41] and expressing the plant F-box protein TIR1 under a ubiquitous promoter (*eft-3*) [42] (referred to as *TIR1; dpy-27::AID*, for complete genotype and allele information for all strains see the Materials and Methods), we were able to time the depletion of DPY-27 by moving worms to auxin-containing plates during or after embryogenesis. To evaluate whether the lack of CEC-4 exacerbates the defects, we also generated a strain containing the *cec-4 (ok3124)* mutation in addition to *TIR1* and *dpy-27::AID* (referred to as *TIR1; dpy-27::AID; cec-4).* For controls, we used wild-type worms (N2), *cec-4* mutants, and a strain with AID-tagged *dpy-27* but no TIR1 expressing transgene (referred to as *dpy-27::AID).*

Our first experiment investigated the ability of embryos exposed to auxin to survive in the absence of DPY-27 throughout the entirety of embryonic development. To ensure that the maternally loaded DPY-27 is also depleted, we initiated our assay at the L4 larval stage of the parent before oocyte production begins **(Fig 1A)** [15]. L4 larvae were placed on auxin-containing plates for a 24-hour egg-laying period, after which the parents were removed. This procedure ensures that both *in-utero* and *ex-utero* development occurs in the presence of auxin. Strains not exposed to auxin were mostly viable, although the *dpy-27::AID*-containing strains had a very low, but statistically significant, level of lethality (**Fig 1B**, Fisher's exact test, p values listed in **S1 File**). While auxin treatment did not significantly impact the survival of control embryos (N2, *cec-4, dpy-27::AID),* 100% of *TIR1; dpy-27::AID and TIR1; dpy-27::AID; cec-4* worms died as embryos or L1 larvae **(Fig 1B)**. These results indicate that DPY-27 function during embryonic development is essential for the survival of hermaphrodite worms, which is consistent with previous studies [39].

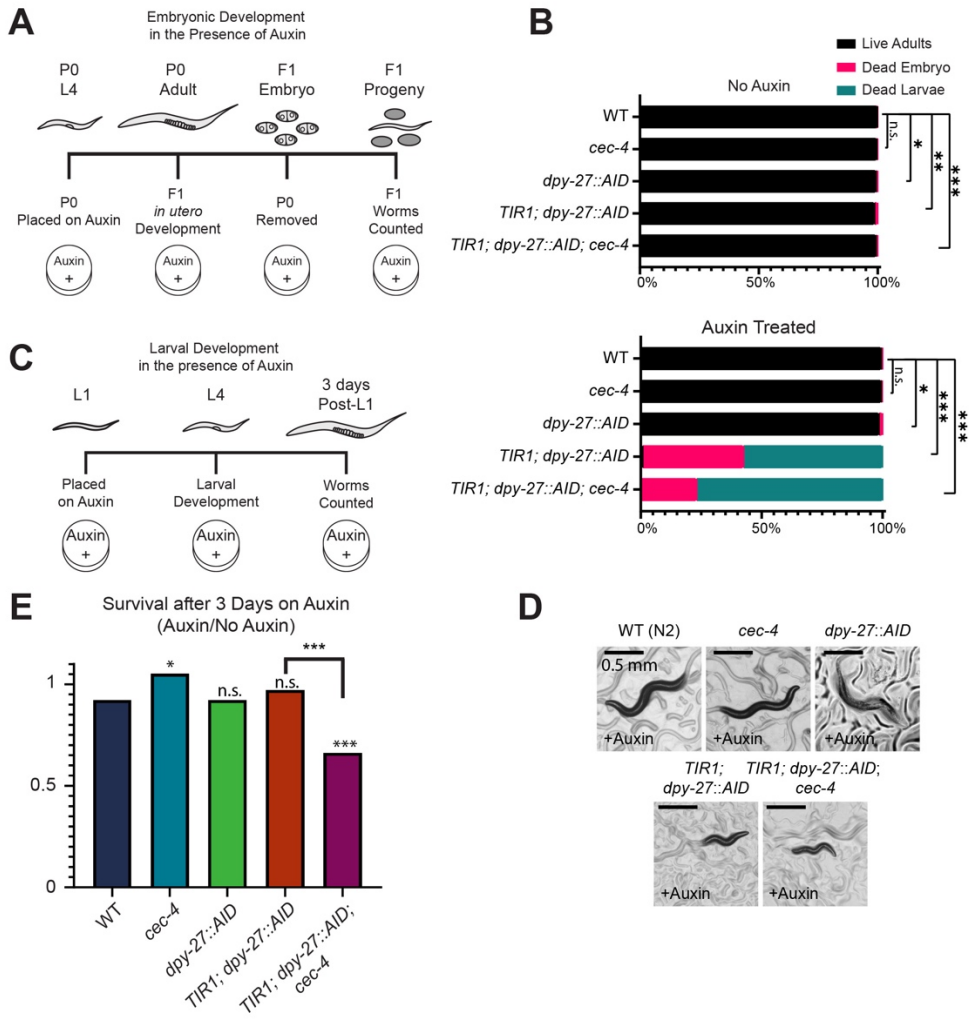

Fig 1. DPY-27 depletion leads to lethality and developmental defects. (A) Overview of the timeline of auxin exposure initiated from parental age L4 through F1 development. **(B)** Auxin exposure throughout embryogenesis results in compromised viability in *TIR1; dpy-27::AID* and *TIR1; dpy-27::AID; cec-4* strains. Significance was determined by Fisher's exact test relative to wild-type values. Dead embryos and dead larvae were summed as one value for statistical analyses. Complete statistical analysis can be found in **S1 File**. **(C)** Overview of the timeline of auxin exposure from the L1 stage for three days. N2 worms in this time frame grow to young adults. **(D)** Phenotypic images of hermaphrodites exposed to auxin from the L1 stage for three days. Scale bar, 0.5 mm. **(E)** Larval survival on auxin relative to survival off auxin. Statistical significance was determined by Chi square tests. Complete statistical analyses can be found in **S2 File**. (n.s. = not significant, * = $p < 0.05$, ** = $p<0.01$, *** = $p < 0.001$).

At the onset of dosage compensation during early embryogenesis, condensin I^{DC} loads onto the X chromosomes in hermaphrodites [15]. However, it is unclear whether the sustained presence of the complex is essential once dosage compensation is

218 established. To assess the requirement for DPY-27 to remain on the X during larval
219 development, we exposed our strains to auxin starting at the L1 larval stage for a period
220 of three days. We compared survival on auxin-containing plates to survival on plates
221 without auxin **(Fig 1C)**. Strains developing without auxin exposure grew to adulthood
222 and produced viable offspring in the timeframe of the experiment. In contrast to
223 embryonic exposure, exposing larvae to auxin had a much lesser effect on survival.
224 Most *TIR1; dpy-27::AID* larvae survived similarly to N2, *cec-4*, or *dpy-27::AID* controls
225 **(Fig 1E,** Chi-square test, p values listed in **S2 File)**. However, DPY-27 depleted strains
226 developed slowly and exhibited developmental defects, including stunted growth **(Fig**
227 **1D)**. The rare embryo produced by these hermaphrodites did not hatch. Adding *cec-4* to
228 the background lowered the survival rate, suggesting that lack of both DPY-27 and
229 CEC-4 results in more severe defects than lack of DPY-27 alone **(Fig 1E)**.

230 Exposure to auxin depletes DPY-27, disrupts DCC binding
231 and H4K20me1 enrichment on the X

232 We next investigated the degree of DPY-27 depletion in auxin-treated strains relative to
233 untreated. DPY-27 was visualized in each strain by immunofluorescence (IF) after
234 worms were exposed to auxin for three days starting at the L1 larval stage. Due to the
235 underdeveloped nature of the DPY-27 depleted strains, we based the timing of IF
236 staining on the growth of wild type. After 3 days, wild-type N2 worms have developed
237 into young adults. IF images were captured in intestinal nuclei. Intestinal cells are 32-
238 ploid and their large size facilitates analyses of the nucleus. Before auxin treatment, all
239 our strains had a wild-type pattern of DPY-27 localization within the nucleus of intestinal
240 cells **(Fig 2A)**, consistent with the lack of any visible defects or lethality in these strains.
241 Auxin treatment in N2, *cec-4*, and *dpy-27::AID* strains led to no observable changes.
242 However, in the *TIR1*-containing strains, *TIR1; dpy-27::AID* and *TIR1; dpy-27::AID; cec-*
243 *4,* auxin treatment resulted in depletion of DPY-27 to background levels **(Fig 2B)**,
244 suggesting that auxin-induced degradation was successful.

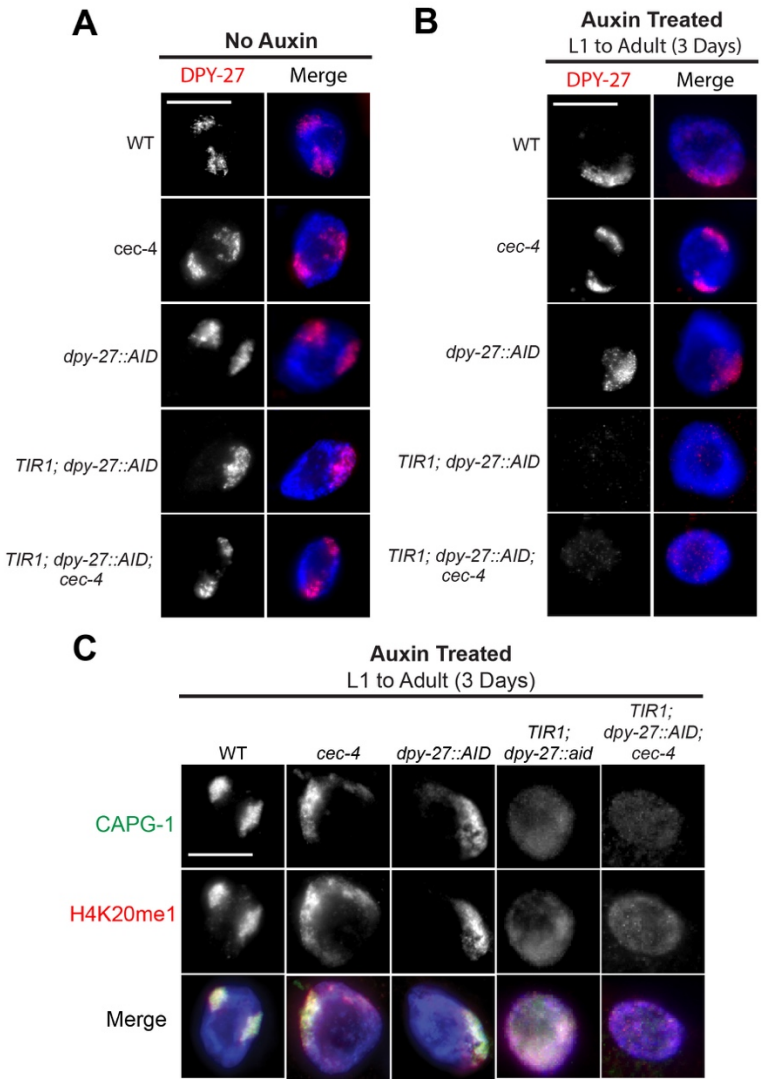

Fig 2. Auxin treatment leads to depletion of DPY-27, loss of DCC binding to the X, and disruption of the X-enrichment of H4K20me1. (A) Immunofluorescence staining of DPY-27 within the intestinal nuclei of young adult hermaphrodites is shown in the left columns, DAPI staining of DNA (blue) is merged with DPY-27 signal (red) in the columns to the right. DPY-27 is present within the nuclei in strains not exposed to auxin. **(B)** Exposure to auxin for 3 days starting at L1 results in a significant depletion of DPY-27 signal (red) by immunofluorescence in strains that contain *TIR1* and *dpy-27::AID* **(C)** DPY-27 depletion from L1 for three days leads to loss of CAPG-1 localization and H4K20me1 enrichment on the X. CAPG-1 (top row, green), H4K20me1 (middle row, red), and a merged image of all three channels, including DAPI DNA staining (bottom row, blue), are shown. **(A-C)** Scale bars, 10 μm.

The observation that *TIR1; dpy-27::AID* and *TIR1; dpy-27::AID; cec-4* larvae can survive despite complete or near complete depletion of DPY-27 prompted us to investigate the degree to which dosage compensation is maintained in these larvae. To assess the binding of other Condensin I^{DC} subunits to the X chromosome following DPY-27

depletion, we performed IF staining for CAPG-1. In N2, *cec-4*, and *dpy-27::AID* strains, CAPG-1 maintains a signal pattern indicative of X chromosome binding. However, in *TIR1; dpy-27::AID* and *TIR1; dpy-27::AID; cec-4,* the CAPG-1 signal becomes non-specific and it diffuses throughout the entire nucleus **(Fig 2C)**. Our results indicate that condensin I^{DC} no longer maintains localization to the X chromosomes following DPY-27 depletion.

We next assessed the enrichment of the histone modification H4K20me1 as a readout for functional DCC binding. In wild-type N2 hermaphrodites, this histone modification is specifically enriched on dosage-compensated X chromosomes [26,27], and this pattern was maintained in *cec-4* and *dpy-27::AID* strains. After exposure to auxin in *TIR1; dpy-27::AID* and *TIR1; dpy-27::AID; cec-4* strains, H4K20me1 was no longer specifically localized within the nucleus, resembling the pattern observed for CAPG-1 localization with the IF signal spread throughout the entirety of the nucleus **(Fig 2C)**. H4K20me1 first becomes enriched on dosage-compensated X chromosomes in mid-embryogenesis [27,36], well before the L1 stage, when auxin treatment was initiated. We conclude that the continued presence of DPY-27 and the DCC is required to maintain this chromatin mark on the X chromosomes. The *TIR1; dpy-27::AID* and *TIR1; dpy-27::AID; cec-4* strains appeared similar in this assay, suggesting that the presence or absence of CEC-4 does not contribute to the maintenance of the H4K20me1 mark.

The continued presence of DPY-27 is required to maintain X chromosome condensation and subnuclear localization

The X chromosomes of wild-type hermaphrodites occupy a surprisingly low proportion of space in the nucleus compared to what is predicted based on DNA content [17]. We previously showed that in DCC mutants and in *cec-4* mutant hermaphrodites, the X chromosomes decondense and relocate toward the more actively transcribed central region of the nucleus [33]. The DCC starts to compact the X chromosomes in early embryogenesis [17]. We tested if the continued presence of DPY-27 is necessary for maintaining the compact conformation and peripheral localization of the X. We performed whole chromosome X paint fluorescence *in situ* hybridization (FISH) to mark the X chromosome territories in intestinal nuclei. Without auxin treatment, the X chromosome signal appeared as expected: compact and near the nuclear periphery in all strains without a *cec-4* mutation and more diffuse in strains with a *cec-4* mutation **(Fig 3A).** After auxin treatment, the X chromosomes appeared enlarged in *TIR1; dpy-27::AID* as well **(Fig 3B)**. We quantified these changes by measuring the proportion of nuclear volume occupied by the X chromosome (see Methods). The X chromosome occupied about 12-13% of the nuclear volume in wild type and close to 20% in *cec-4* mutants **(Fig 3C, S3 File** for complete statistical analysis**)**, which is consistent with previous results [33]. In the *TIR1; dpy-27::AID* strain, depletion of DPY-27 led to decondensation of the X chromosome to a degree similar to *cec-4* mutants or to what was previously observed in worms treated with *dpy*-27 RNAi [17]. These findings demonstrate the critical role of DPY-27 in maintaining the compact conformation of the

X chromosome in wild-type hermaphrodites. In the *TIR1; dpy-27::AID; cec-4* strain, the X was already decondensed without auxin treatment due to the presence of the *cec-4* mutation, and depletion of DPY-27 led to a measurable level of additional decondensation **(Fig 3C)**. These results indicate that the presence of DPY-27 maintains X compaction, and the additional loss off *cec-4* exacerbates decondensation.

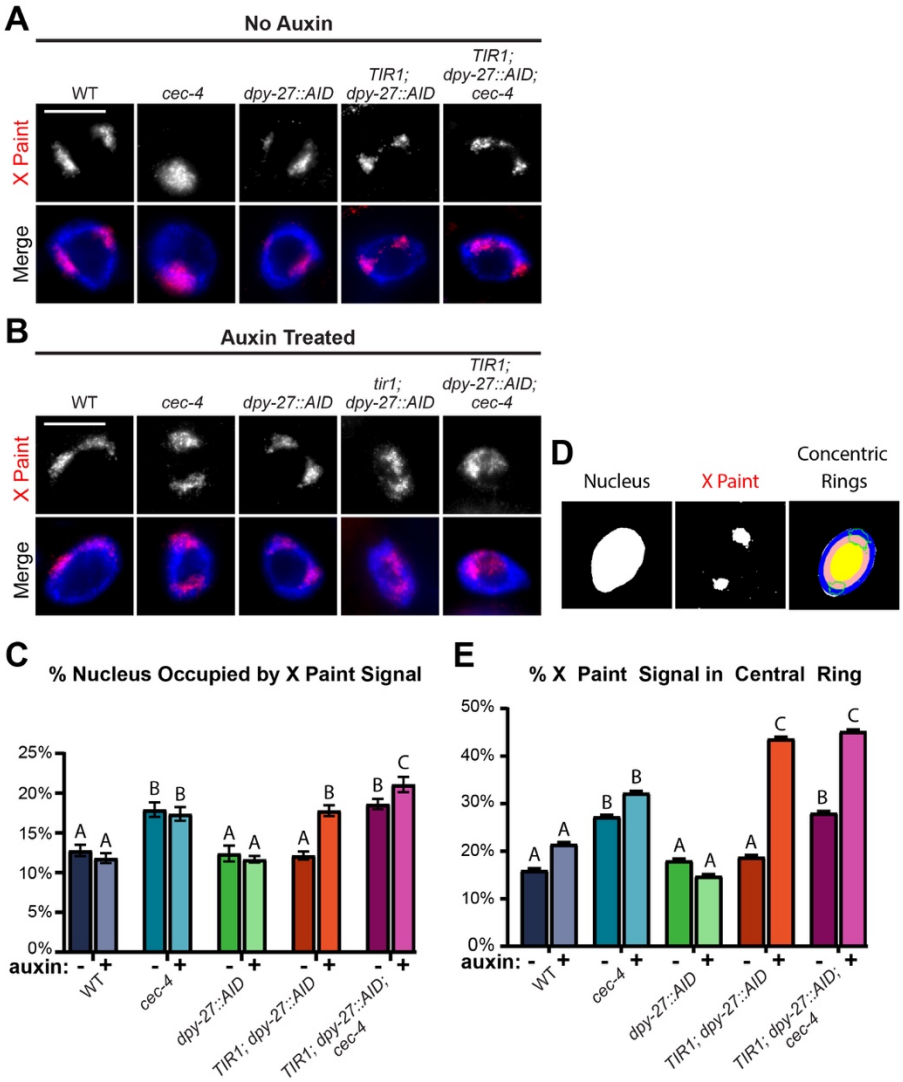

Fig. 3 The continued presence of DPY-27 is required for X compaction and peripheral localization within the nucleus. (A) Intestinal nuclei from adult hermaphrodites not exposed to auxin were stained with whole X chromosome paint FISH probe (top row, red), and DNA was labeled with DAPI (blue). Representative images are from young adult 3 days post-L1 hermaphrodites not exposed to auxin. **(B)** X chromosome paint FISH was performed in intestinal cells of hermaphrodites exposed to auxin from L1 for three days. **(C)** Quantifications of the X chromosome volume normalized to nuclear size (n = 20 nuclei). Hermaphrodites grown without auxin are indicated by "-", and auxin-treated worms are designated by "+". *dpy-27* depletion or *cec-4* mutation increases X decondensation. For complete statistical analysis see

S3 File. (D) Three-zone assay segmenting shown on a single slice from the middle of an intestinal nucleus. The amount of X signal (outlined in green) in each ring was quantified. **(E)** The proportion of the X paint signal seen in the central zone of the nucleus (n = 20 nuclei). Relocation to the center of the nucleus is increased DPY-27 depleted worms or *cec-4* mutants. Hermaphrodites grown without auxin are indicated by a "-" (bars on the left), and auxin-treated worms are designated by a "+". For complete statistical analysis see **S4 File. (A-B)** Scale bars, 10 μm. **(C, E)** Values sharing the same letter are considered statistically not different from each other (n.s. = $p>0.05$). Distinct letters indicate significant differences between the corresponding values ($p<0.05$, Student's t-test). Error bars indicate the standard error of the mean. Complete signal analyses in all concentric rings can be found in **Fig S1.**

Dosage compensation mechanisms makes the X chromosomes not only compact but also position the chromosomes near the nuclear periphery [33]. To assess any changes in subnuclear localization, we analyzed our X chromosome FISH signals in the various strains using a three-zone assay (see Methods) **(Fig 3D).** The localization of the X within the nucleus was assessed in three concentric zones, and the portion of the X signal in the central zone was quantified from a single focal plane taken from the middle of the nucleus. **(Fig 3D)**. In wild-type hermaphrodites, we observed the expected X localization. Only a small portion of the signal reaches into the center ring, while the bulk of the X is located in the intermediate and peripheral zones of the nucleus **(Fig 3E, S1 Fig, S4 File** for complete statistical analysis**),** as observed before [33]. In *cec-4* mutants (*cec-4* and *TIR1; dpy-27::AID; cec-4)*, significantly more of the X signal is in the center, as expected. The relocation is even more significant in DPY-27 depleted strains **(Fig 3E)**. In both *TIR1; dpy-27::AID* and *TIR1; dpy-27::AID; cec-4* strains, over 40% of the signal is localized in the central region, suggesting that the depletion of DPY-27 has a more significant impact on X nuclear localization than the *cec-4* mutation. Adding *cec-4* mutation did not significantly increase the degree of movement to the middle region compared to DPY-27 depletion alone. Overall, these data indicate that the continued presence of DPY-27 is required to maintain X compaction and peripheral localization and that adding a *cec-4* mutation led to further X decompaction but no additional relocalization to the central zone of the nucleus.

The continued presence of DPY-27 is required in fully differentiated postmitotic cells

Thus far, we analyzed worms for which the auxin treatment began at the L1 larval stage and ended 3 days later (the duration of time in which N2 reaches adulthood). In this timeframe, intestinal nuclei undergo 4 rounds of endoreduplication and reach the stage of 32-ploidy [43]. To analyze the continued need for DPY-27 after these altered cell cycles have taken place and the cells have fully differentiated, we performed experiments where the auxin treatment began in adulthood (3 days past L1). The auxin-degron system is very effective in *C. elegans,* with protein degradation observable within 30 minutes [42]. We subjected adult hermaphrodites to auxin for one hour to assess whether one hour was sufficient for DPY-27 degradation. In *TIR1; dpy-27::AID*

360 and *TIR1; dpy-27::AID; cec-4* strains, we observed significant protein depletion,
361 comparable to longer treatments, as visualized by IF staining **(Fig 4A)**.

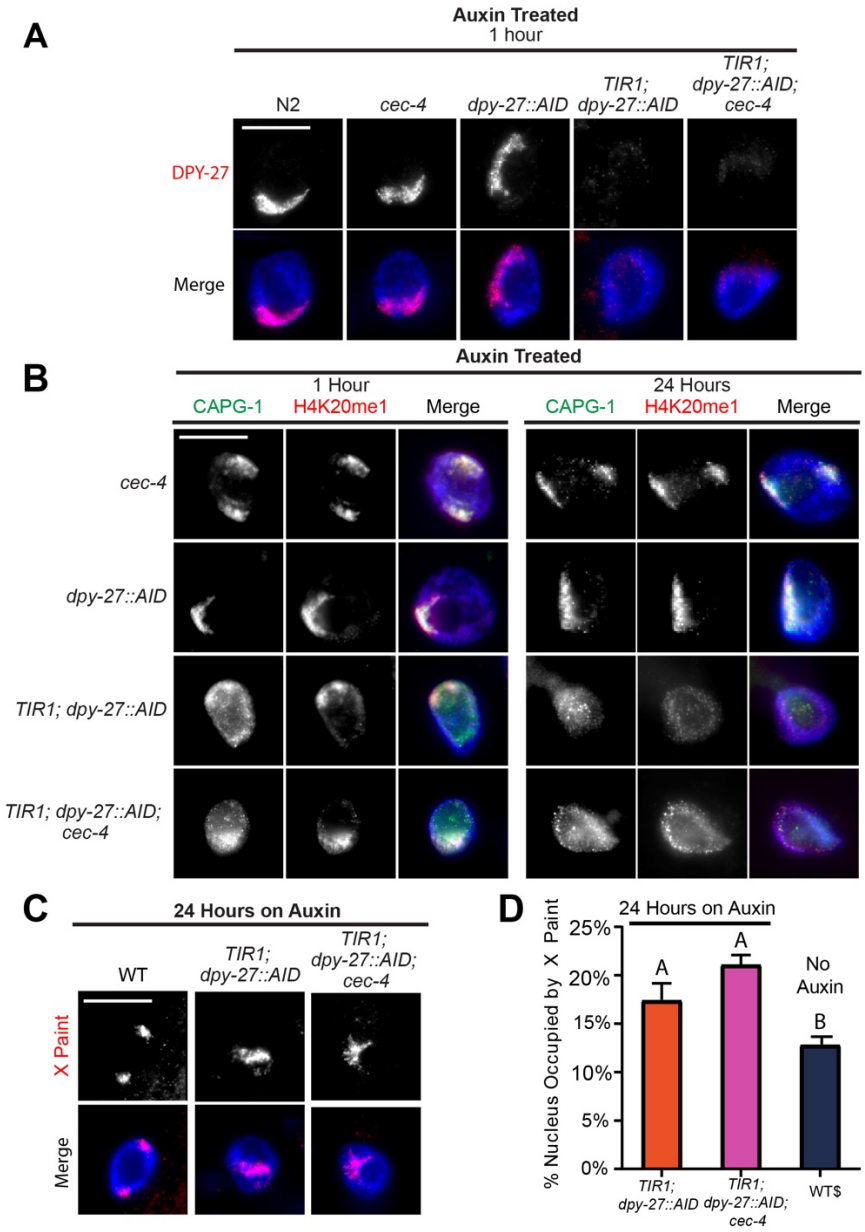

362

363 **Fig 4. Rapid depletion of DPY-27 leads to a subsequent gradual loss of CAPG-1 and**
364 **H4K20me1 enrichment on the X. (A)** Young adult hermaphrodites were exposed to auxin for
365 one hour before dissection, fixation, and IF staining for DPY-27 (red) and DNA (DAPI, blue).
366 DPY-27 signal was significantly depleted in *TIR1; dpy-27::AID* and *TIR1; dpy-27::AID; cec-4*
367 strains **(B)** Immunofluorescent analysis of young adult hermaphrodites using antibodies for
368 CAPG-1 (green) and H4K20me1 (red) after auxin exposure for one hour (columns on the left)
369 and 24 hours (columns on the right). **(C)** X paint FISH (red) staining of adult *TIR1; dpy-27::AID*
370 and *TIR-1; dpy-27::AID; cec-4* after 24-hours of auxin exposure. **(D)** Quantification of the
371 volume of the X paint FISH signal. Significance was determined by Student's t-test. Values
372 sharing the same letter are not significantly different. Distinct letters indicate significant

373 differences between the corresponding values ($p<0.05$). WT data ($) is repeated from Fig 3C.
374 Error bars indicate the standard error of the mean. **(A-D)** Scale bars, 10 μm.

375

376 Given the rapid depletion of DPY-27, we investigated potential alterations in
377 mechanisms linked to dosage compensation. To assess whether H4K20me1
378 enrichment is sustained after DPY-27 loss, intestinal nuclei of young adult
379 hermaphrodites exposed to auxin for one hour were stained with an antibodies targeting
380 H4K20me1 and the DCC subunit CAPG-1. Auxin exposure for one hour resulted in the
381 CAPG-1 signal appearing diffuse throughout the nucleus in *TIR1; dpy-27::AID* with and
382 without *cec-4*, but with partial enrichment over a portion of the nucleus, presumably the
383 X chromosome **(Fig 4B, left)**. These results indicate that after DPY-27 depletion, the
384 rest of the DCC also rapidly dissociates from the X, but with a slight delay compared to
385 the DPY-27. Notably, H4K20me1 staining also appeared somewhat limited to this
386 region but more diffuse than in controls. Strains in which DPY-27 was not depleted (*cec-*
387 *4* and *dpy-27::*AID) exhibited a clear overlap of the H4K20me1 and the CAPG-1 signals,
388 comparable to no auxin controls. However, the changes in staining of H4K20me1 and
389 CAPG-1 after one hour of auxin treatment are not as drastic as in hermaphrodites
390 exposed to auxin for three days. To test whether prolonged exposure would lead to
391 more complete loss of enrichment, we exposed young adult hermaphrodites to auxin for
392 24 hours. After 24 hours, *TIR1; dpy-27::AID* and *TIR1; dpy-27::AID; cec-4* exhibited a
393 complete loss of the X-enrichment of the CAPG-1 and H4K20me1 signals **(Fig 4B,**
394 **right)**, indistinguishable from results obtained with worms treated with auxin for three
395 days of larval development **(Fig 2C)**. We performed whole X paint FISH on strains
396 exposed to auxin for 24 hours **(Fig 4C)**. We observed X chromosome decondensation
397 to levels similar to worms exposed to auxin for 3 days **(Fig 4D)**. Hence, we conclude
398 that the continued presence of DPY-27 is required to maintain the dosage-compensated
399 state even in fully differentiated postmitotic cells and that depletion of DPY-27 leads to
400 the rapid loss of features associated with dosage compensation.

401 X-linked genes are derepressed after DPY-27 depletion

402 We next tested whether these changes in X chromosome compaction, nuclear
403 organization, and the depletion of repressive histone marks, led to increases in X
404 chromosome gene expression in the *TIR1; dpy-27::AID* and *TIR1; dpy-27::AID; cec-4*
405 strains when treated with auxin. Although nuclear organization and H4K20me1
406 enrichment were not significantly different with and without a mutation in *cec-4*, the
407 reduced viability of auxin-treated *TIR1; dpy-27::AID; cec-4* larvae compared to *TIR1;*
408 *dpy-27::AID* larvae also suggested that the X may be more derepressed in the strain
409 also lacking *cec-4.* To test these hypotheses, we extracted total mRNA from
410 synchronized L3 populations, which were grown in the presence of auxin starting at L1
411 or grown in the absence of auxin for controls. We performed these experiments at the
412 L3 stage rather than at a later stage, because at this stage the delay in growth and
413 development of the DPY-27 depleted strains is not yet apparent, and also to avoid

414 complications arising from the contributions from the germline where the X
415 chromosomes are subject to regulation unrelated to dosage compensation [44]. At the
416 L3 stage, the germline consists of only about ~60 cells, and thus the RNA extracted
417 from whole worms represents predominantly somatic tissues [45]. The mRNA-seq
418 readout is plotted as a log2-fold change in gene expression on autosomes and the X in
419 auxin-treated samples compared to controls **(Fig 5, Fig S2, S5 File).**

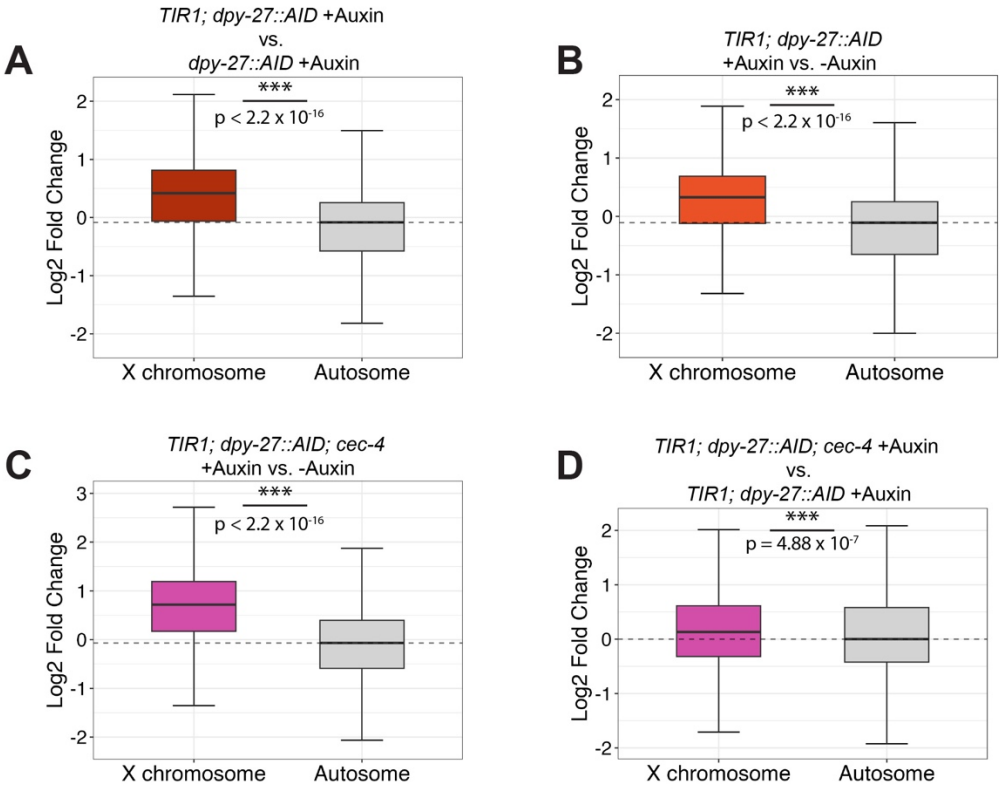

420

421 **Fig 5. The X-linked gene expression is derepressed in strains depleted of DPY-27. (A-D)**
422 Boxplots depicting the distribution of the log2 fold change of the X-linked genes and of the
423 autosomal genes in strains being compared. A Wilcoxon rank-sum test was used to determine
424 the statistical significance of the differential gene expression between the X and autosomes.
425 (n.s. = not significant, * = p < 0.05, ** = p<0.01, *** = p < 0.001) **(A)** The log2 fold change in gene
426 expression of the autosomes and the X chromosomes of *TIR1; dpy-27::AID* relative to the *dpy-*
427 *27::AID* after both strains were exposed to auxin. **(B)***TIR1; dpy-27::AID* treated with auxin
428 compared to the same genotype grown in the absence of auxin. **(C)** *TIR1; dpy-27::AID; cec-4*
429 treated with auxin was compared to no auxin treatment. **(D)** *TIR1; dpy-27::AID; cec-4* compared
430 to *TIR1; dpy-27::AID,* both treated with auxin.

431

432 Without exposure to auxin, the *dpy-27::AID* strain had similar gene expression levels to
433 N2, although the slight X derepression was statistically significant. The minimal change
434 in gene expression suggests that tagging DPY-27 with the degron tag did not
435 significantly disrupt its function **(Fig S2A)**. *cec-4* strains treated with auxin also
436 displayed slight X depression compared to *cec-4* mutants without auxin exposure,

437 indicating a minimal influence of auxin treatment on gene expression regulation **(Fig**
438 **S2B)**. The *TIR1; dpy-27::AID* and the *TIR1; dpy-27::AID; cec-4* strains also had a small
439 degree of X derepression compared to wild type even in the absence of auxin, possibly
440 due to somewhat leaky *TIR1* activity (**Fig S2C and D**), which is a phenomenon noted by
441 other research groups as well [46–48]. Therefore, to assess the increase in X-linked
442 gene expression resulting the loss of DPY-27, we compared gene expression levels in
443 the same strain with and without auxin and/or in auxin-treated strains with and without
444 TIR1 expression **(Fig 5)**. In comparison to *dpy-27::AID*, the strain *TIR1; dpy-27::AID* had
445 significant upregulation of the X chromosome when treated with auxin, while autosomal
446 gene expression remained unchanged (X derepression (defined as median X-linked
447 log2 fold change – median autosomal log2 fold change) = 0.503) **(Fig 5A)**. Similarly,
448 auxin-treated *TIR1; dpy-27::AID* exhibited significant X derepression (0.435) compared
449 to non-auxin-treated **(Fig 5B)**. These results demonstrate that depletion of DPY-27
450 during the maintenance phase of dosage compensation leads to significant X
451 derepression .

452 We then investigated whether the absence of CEC-4 further enhanced X derepression.
453 Comparing the mRNA-seq gene expression profiles of *TIR1; dpy-27::AID; cec-4* treated
454 with auxin to untreated populations of the same genotype, we observed a significant
455 increase in X-linked gene expression (0.78) **(Fig 5C)**. The degree of X derepression
456 was greater than that caused by auxin treatment in *TIR1; dpy-27::AID* without the *cec-4*
457 mutation. These results suggest that the loss of *cec-4* may exacerbate X dosage
458 compensation defects. To confirm, we compared *TIR1; dpy-27::AID; cec-4* to *TIR1; dpy-*
459 *27::AID* after auxin treatment. The difference between these two populations was
460 substantial (0.13), suggesting that depletion of DPY-27 leads to a greater level of X
461 derepression in a strain that lacks CEC-4 **(Fig 5D)**. These results are consistent with
462 CEC-4 playing a supporting role in helping to maintain stable X chromosome repression
463 in differentiated cells.

464 Loss of *cec-4* activity exacerbates dosage compensation 465 defects caused by a mutation in *dpy-21*

466 Our experiments showed that the loss of CEC-4 sensitizes hermaphrodite *C. elegans* to
467 dosage compensation defects caused by DPY-27 depletion **(Fig 5D)**. To test whether
468 loss of CEC-4 also exacerbates defects caused by other dosage compensation
469 mutations, we sought to understand the interplay between CEC-4, known for its role in
470 tethering the X chromosomes to the nuclear lamina [33], and DPY-21, whose activity
471 leads to X-specific enrichment of H4K20me1 [25]. Individually, the mutations in these
472 pathways lead to phenotypes related to dosage compensation defects and changes in
473 X-linked gene expression, but despite these changes, the mutants are viable
474 [22,25,26,32,33]. Since *dpy-21* null mutants (*dpy-21(e428))* are viable [22], we
475 performed these experiments with the null mutant rather than using the AID system.
476 Therefore, our experiment tested the impact of these mutations throughout the lifespan
477 of the animals, including both the establishment and the maintenance phases of dosage

compensation. We constructed a double mutant *cec-4 (ok3124)* IV*; dpy-21(e428)* V strain (referred to as *cec-4; dpy-21).* The strain is viable but with visible defects, such as a Dpy phenotype.

We first evaluated the ability of hermaphrodites lacking functional *cec-4* and *dpy-21* to lay viable eggs. The total number of eggs laid by *cec-4; dpy-21* hermaphrodites was significantly smaller than all other strains observed, including the *dpy-21* and *cec-4* single mutants **(Fig 6A)**. In all strains, most embryos hatched into larvae within 24 hours (**Fig 6B**). Most wild-type (N2) and *cec-4* mutant larvae developed into adulthood. While the viability of *dpy-21* mutant larvae was somewhat reduced, it was not significantly different from the viability of *cec-4; dpy-21* double mutants **(Fig 6C).** Overall, these results suggest that the addition of the *cec-4* mutation does decrease the overall fitness of *dpy-21* mutants.

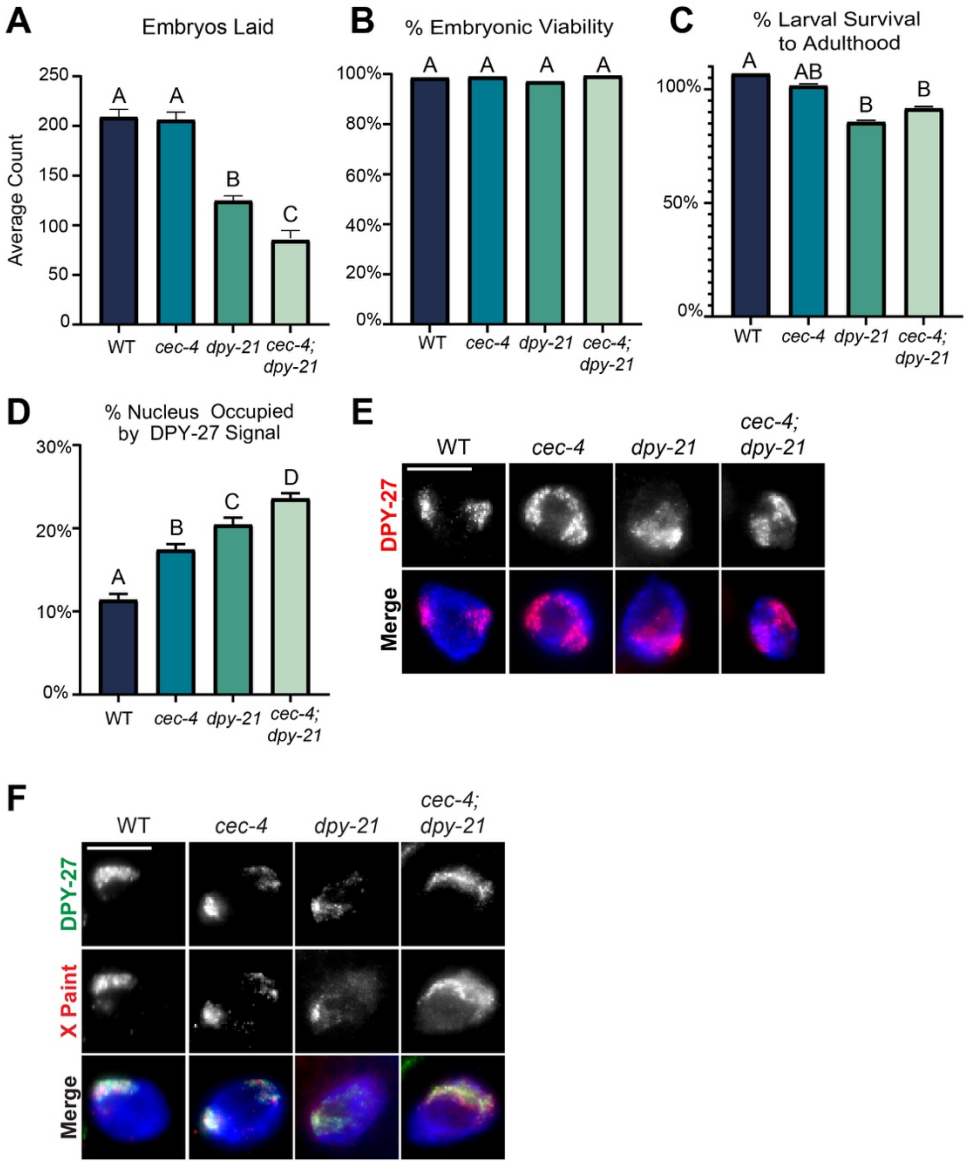

Fig 6. Loss of CEC-4 exacerbates dosage phenotypes caused by mutations in dpy-21.(A) The average of total number of eggs laid. A mutation in *dpy-21* decreases the average brood size. The double mutant, *cec-4; dpy-21*, yields the smallest brood. **(B)** The average percentage of embryos that hatched after 24 hours (hatched embryo after 24 hours/total embryo). **(C) The average percentage of larvae that survived to adulthood.** The few embryos laid by the *cec-4; dpy-21* strain can survive to adulthood but at a frequency lower than that of the wild type. **(A-C)** The error is reported as the standard error of the mean (n = 6-8 hermaphrodites). For statistical analysis see S6 File. **(D)** The extent of X chromosome decompaction. Error bars represent standard error of mean (n = 20). For statistical analysis, see S7 file. **(E)** Representative images of adult hermaphrodite intestinal nuclei stained for DPY-27 (top, red) and DNA (bottom, DAPI, blue). **(F)** DPY-27 (green) co-localizes to the X paint FISH signal (red) in all assayed strains. **(E, F)** Scale bar, 10 μm. **(A-D)** Values sharing the same letter are considered not statistically significantly different (n.s. = p>0.05). Distinct letters indicate significant differences between the corresponding values (p<0.05, Student's t-test).

We employed DPY-27 staining to mark the X chromosomes to assess the level of X chromosome compaction. All mutants exhibited a prominently decondensed X chromosome **(Fig 6E)**. Further quantitative analysis revealed that the X chromosomes were decondensed in *cec-4* and *dpy-21* single mutants, but in the *cec-4; dpy-21* double mutant strain the X occupied an even more significant proportion of the nucleus **(Fig 6D)**. The localization of DPY-27 to the X chromosome was not influenced by the loss of *cec-4* and/or *dpy-21* **(Fig 6F)**. These observations show that adding the *cec-4* mutation to *dpy-21* mutants augments some defects associated with dosage compensation.

To determine the impact of these mutations on X chromosome gene repression, mRNA-seq was performed in L3 hermaphrodites **(Fig S3,** See **S5 File** for statistical analysis**)**. We previously reported subtle upregulation of the X chromosomes in *cec-4* mutant L1 larvae compared to the wild type [33]. In L3 larvae, this upregulation was even more modest and not statistically significant (X derepression = 0.027, p = 0.421) **(Fig 7A)**, suggesting that lack of CEC-4 alone does not have a significant impact on X-linked gene regulation despite the observed changes in X chromosome compaction and nuclear localization. In contrast, the *dpy-21* mutant displayed a more pronounced derepression of the X chromosome (0.612, $p < 2.2 \times 10^{-16}$) **(Fig 7B)**, consistent with previous results [25,29]. When we compared the *cec-4; dpy-21* double mutant to the wild type, we observed an even more drastic change in gene expression (X depression = 0.721, $p = 2.2 \times 10^{-16}$) **(Fig 7C)**. Furthermore, when juxtaposing the *cec-4; dpy-21* double mutant against its single mutant counterparts, the results underscored that *cec-4; dpy-21* expressed X-linked genes at a higher level than either single mutant (*cec-4; dpy-21* vs *cec-4* : X derepression = 0.669, $p = 2.2 \times 10^{-16}$, and *cec-4; dpy-21* vs *dpy-21*: X derepression = 0.09, $p = 5.05 \times 10^{-13}$) **(Fig 7D** and **E)**. Given the relatively minor derepression of the X chromosome in *cec-4* mutants, a significant increase in the X-linked gene expression levels of *cec-4; dpy-21* compared to *cec-4* alone was expected **(Fig 7D)**. The *dpy-21* single mutant already exhibited an upregulation in X chromosome gene expression; however, the *cec-4; dpy-21* double mutant significantly surpassed it in X derepression **(Fig 7E)**. While *cec-4*, as a single mutation, does not substantially

impact X-linked gene expression, our results show that the loss of *cec-4* sensitizes hermaphrodites to additional dosage compensation defects.

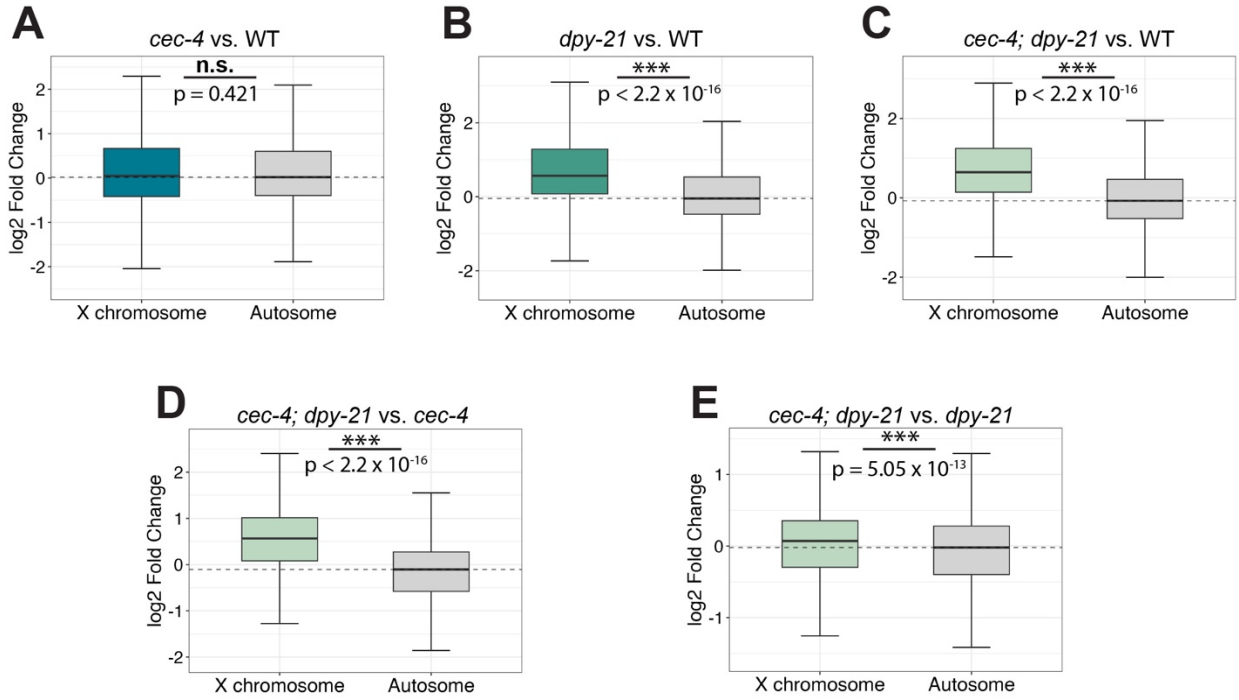

Fig 7. Loss of CEC-4 exacerbates gene expression defects caused by mutations in *dpy-21*. (A-E) Boxplots depicting the distribution of the expression of X-linked genes and expression of genes on autosomes. Gene expression is plotted as the log2 fold change of the strains being compared. Statistical significance is determined by the differences in gene expression between the X and autosomes by a Wilcoxon rank-sum test. (n.s. = not significant, * = $p < 0.05$, ** = $p<0.01$, *** = $p < 0.001$) **(A)** The log2 fold change in gene expression of the autosomes and the X chromosomes in *cec-4* mutant relative to the wild type (N2). **(B)** The log2 fold change in gene expression of the autosomes and the X chromosomes in *dpy-21* mutants relative to wild type (N2). **(C)** The log2 fold change in gene expression in *cec-4; dpy-21* relative to wild type (N2). **(D)** The log2 fold change in gene expression in *cec-4; dpy-21* compared to *cec-4*. **(E)** The log2 fold change in gene expression in *cec-4; dpy-21* compared to *dpy-21*. The derepression of the X chromosome genes is significantly higher in the double mutant than in single mutants.

Discussion

In this study, we investigated the relative contributions of the DCC to two phases of dosage compensation: establishment and maintenance. We depleted DPY-27, a core protein subunit of the dosage compensation machinery, condensin I^{DC}, using the auxin-inducible degron system during embryonic and larval development. Our data indicated that DPY-27 function is essential during embryonic development, but the protein is dispensable for hermaphrodite survival during larval and adult stages. In an additional dosage compensation mechanism, the non-condensin DCC member DPY-21 significantly contributes to X-linked gene repression by enriching H4K20me1 on the X chromosome [25]. We show that the enrichment of H4K20me1 is lost rapidly after DPY-27 depletion, indicating that the mark must be continuously maintained, presumably by

561 DPY-21 recruited to the X by DPY-27. In addition, DPY-27 depletion leads to X
562 chromosome decondensation and relocation to a more central position in the nucleus,
563 as well as significant increases in X-linked gene expression. In addition to the
564 contributions of the DCC, nuclear lamina association of the X chromosome via
565 H3K9me3 binding to CEC-4 also contributes to X morphology and repression [33]. We
566 found that a loss-of-function mutation in *cec-4* amplifies the sensitivity of
567 hermaphrodites to the depletion/mutation of other dosage compensation processes.
568 These results suggest that nuclear lamina anchoring by CEC-4 serves to stabilize
569 repression initiated by condensin I^{DC} or H4K20me1. By loss-of-function mutations in
570 *cec-4* and *dpy-21* and depletion of DPY-27, we unexpectedly revealed that larval and
571 adult hermaphrodites are resilient to depletion of known dosage compensation
572 mechanisms and substantial increase in X-linked gene expression.

573 Condensin I^{DC} function is required for embryonic viability but not for 574 larval and adult viability

575 A previous study using a cold-sensitive mutant for *dpy-27* demonstrated that inactivating
576 DPY-27 during the comma stage of embryonic development leads to more extensive
577 lethality than inactivation of the protein at later stages. However, the differences in
578 viability counts at the different temperatures were only about 20% [39]. We re-examined
579 this question using the auxin-mediated degradation system, where adding auxin leads
580 to rapid and near complete depletion of DPY-27. Prior to auxin treatment, the strains
581 had essentially 100% viability, while auxin treatment during embryogenesis led to
582 essentially 100% lethality. These results demonstrate that condensin I^{DC} activity is
583 essential during embryonic development when cell fates are being specified, and cells
584 begin to differentiate into different cell types. At the end of embryonic development, the
585 embryo consists of about 500 cells, the majority of which have exited the cell cycle and
586 begun terminal differentiation [38]. Depletion of condensin I after embryogenesis is not
587 incompatible with viability despite developmental abnormalities in depleted larvae. This
588 result raised two possibilities. First, it is possible that dosage compensation, once
589 established, can be maintained in the absence of condensin I^{DC}. Second, it is possible
590 that X chromosome repression is not maintained but the larvae can tolerate defects in
591 X-linked gene regulation. Our results, discussed below, are consistent with the second
592 scenario.

593 Condensin I^{DC} must remain on the X to maintain the condensed 594 conformation

595 We show that compaction of the dosage compensated X cannot be maintained without
596 DPY-27. By varying durations of auxin exposure and observing the condensin I^{DC}
597 subunit CAPG-1, we saw the gradual loss of of condensin I^{DC} enrichment on the X **(Figs**
598 **2 and 4)**. We propose that the absence of DPY-27 leads to the destabilization of the
599 condensin I^{DC} ring, resulting in the eventual release of the complex from the X. The X
600 chromosome also decondenses after condensin I^{DC} loss, indicating that chromosome
601 compaction must be actively maintained. Previous research investigating the

602 maintenance of mitotic or meiotic chromosome architecture demonstrated that
603 depletion or inactivation of mitotic condensin subunits after chromosome condensation
604 has taken place leads to disorganized chromosome structure with reduced rigidity or a
605 larger surface area [49–52]. Similar to what we observed about the continued need for
606 condensin I^{DC} to maintain the compact structure of dosage compensated X
607 chromosomes, maintenance of mitotic chromosome architecture also requires the
608 continued presence of condensin. However, in the studies of mitotic chromosomes,
609 compaction was maintained after condensin loss, only the organization or rigidity of
610 chromosomes was altered. In our study, the interphase X chromosome was was not
611 maintained. It has been suggested that during mitosis additional mechanisms, such as
612 posttranslational histone modifications, contribute to chromosomes condensation [53].
613 We hypothesize that in the absence of these mitosis-specific histone modifications in
614 interphase, condensin function is necessary for compaction. We note that two
615 posttranslational histone modifications associated with mitosis, namely enrichment of
616 H4K20me1 and depletion of H4K16ac, are also features of interphase dosage
617 compensated X chromosomes of *C. elegans* [26,27,53–55]. However, additional mitotic
618 histone modifications that are not present on dosage compensated X chromosomes (for
619 example H3S10Ph or depletion of additional acetylation marks) may also contribute to
620 condensin independent chromosome compaction in mitosis [56]. Our findings indicate
621 that the complete condensin complex must remain associated with the X for the
622 maintenance of compaction during developmental stages in which most cells are post-
623 mitotic. It will be interesting to investigate the maintenance of chromosome architecture
624 changes on dosage compensated Xs at higher resolution, such as formation of TADs
625 using Hi-C.

626 The presence of DPY-27 is required to actively maintain the 627 enrichment of H4K20me1 on the X

628 Concurrently with the loss of CAPG-1 signal, the H4K20me1 mark exhibits a loss of
629 specific localization on the X with increasing auxin exposure time **(Figs 2 and 4)**. We
630 propose that the continued presence of DPY-21 (presumable recruited by DPY-27) on
631 the X is necessary to maintain H4K20me1 enrichment on the X. Notably, the presence
632 of DPY-21 is not essential for the localization of condensin I^{DC} on the X; however, for
633 DPY-21 to bind the X, the presence of condensin I^{DC} is required [22]. Our results are
634 similar to what was seen for H3K9me2 and MET-2. Maintenance of this chromatin mark
635 in *C. elegans* also requires the continued presence of the enzyme that places it [57].
636 Our results suggest that functional Condensin I^{DC} plays a role in maintaining the
637 localization of DPY-21 on the X, and its continued presence is required even in post-
638 mitotic developmental stages. We hypothesize that in the absence of DPY-27 and DPY-
639 21, either there is frequent enough histone turnover to lose the H4K20me1 enrichment
640 or that the X is rendered accessible to histone modifiers that remove the H4K20me1 or
641 modify the mark to di- or trimethylation.

642 **Condensin I^{DC} is required to maintain X-linked gene repression in**
643 **hermaphrodites**
644 Severe depletion or mutation of dosage compensation in *C. elegans* is hermaphrodite
645 lethal. Unexpectedly, we observed that hermaphrodites survive as larvae with severe
646 depletion of DPY-27, albeit with major phenotypic defects **(Fig 1C).** Furthermore**,** they
647 survive without other vital contributors to X-linked gene regulation in addition to DPY-27
648 depletion, namely, nuclear lamina tethering by CEC-4 and H4K20me1 **(Fig 2C)**. In
649 short, auxin-treated *TIR1; dpy-27::aid; cec-4* larvae survive without measurable activity
650 of any known dosage compensation mechanism. Our study revealed increases in X-
651 linked gene expression beyond levels reported in *dpy-27* null mutant embryos or L1
652 larvae (log2 fold change in X-linked gene expression of less than 0.3) [29] or *sdc-2*
653 mutant embryos treated with *sdc-2* RNAi (log2 fold change about 0.6) [58]. Dosage
654 compensation defects in these mutants lead to lethality. Our most significant increase in
655 X-linked gene expression was measured in *TIR1*; *dpy-27::AID; cec-4* L3 larvae after
656 auxin exposure with a log2 fold change in X-linked gene expression at a value of 0.78
657 **(Fig 5)**. These larvae survive despite more significant gene expression defects than
658 previously reported for embryos dying of dosage compensation defects. We suggest
659 that the absence of these dosage compensation processes is acceptable in these
660 animals because the continued repression of the X is no longer essential after early
661 development once cell fates have been specified and the cells have differentiated.

662 In mice, the critical contributor to dosage compensation, the long non-coding RNA *Xist*,
663 can be deleted with minimal change to X repression as long as it is deleted during the
664 maintenance phase after X chromosome inactivation is fully established [59,60].
665 However, unlike the continued repression of the mouse X despite the loss of *Xist*, we
666 observed a significant derepression of X-linked genes in *C. elegans* hermaphrodites
667 after the depletion of DPY-27. The difference might be due to the nature of the
668 repressive mechanisms. In mice, X chromosome inactivation involves the establishment
669 of facultative heterochromatin on the X chromosomes, including DNA methylation and
670 heterochromatic histone modifications [61]. Studies in other organisms have shown that
671 these chromatin marks can be maintained by propagating them during the S phase [62–
672 65], even without the initial trigger. The repressive mechanisms involved in *C. elegans*
673 dosage compensation are different. H4K20me1 patterns are not propagated during
674 DNA replication; in fact, H4K20me1 levels decrease in S phase due to the activity of an
675 H4K20me1 demethylase PHF8 [66]. Instead, H4K20me1 is thought to be established
676 during mitosis [54] and then converted to H4K20me2/3 methylation after mitotic exit
677 [54]. Our results suggest that maintenance of this mark on dosage compensated X
678 chromosomes requires the continued presence of DPY-27, presumably recruiting the
679 H4K20me2 demethylase DPY-21 [25].

680

The loss of function of cec-4 sensitizes hermaphrodites to the loss of DPY-27 or DPY-21

The *cec-4* mutation, combined with DPY-27 depletion, showed only minor changes in nuclear compartmentalization and chromosome compaction compared to DPY-27-depleted strains with functional CEC-4 (**Figs 3** and **4)**. However, there was a notable decrease in hermaphrodite viability of DPY-27 depleted larvae with a *cec-4* mutation compared DPY-27 depleted larvae without a *cec-4* mutation (**Fig 1E**), suggesting disruption to X-linked gene regulation approaching unacceptable limits for survival. When a *cec-4* mutation was combined with a *dpy-21* mutation, there was an observable increase in X decompaction and a decrease in brood size in the double mutant compared to single mutants, again suggesting greater disruption to dosage compensation (**Fig 6**). mRNA-seq analysis indicated that the loss-of-function mutation of *cec-4* alone minimally increased X-linked gene expression **(Fig 7A)**. However, in scenarios where a *cec-4* mutation was coupled with DPY-27 depletion or *dpy-21* mutation, we observed a substantial increase in X-linked gene expression, significantly more than in strains without the *cec-4* mutation **(Figs 5,** and **7)**. Previous studies have highlighted the involvement of CEC-4 in cellular differentiation and stabilizing cell fates [32]. Cells actively undergoing differentiation demand precise gene expression levels. However, we hypothesize that the loss of some repressive mechanisms after differentiation are acceptable, partly because CEC-4 may help lock down established gene expression patterns, including the repressed state of dosage-compensated X chromosomes. It should be noted, however, that the loss of *cec-4* challenges the health of *C. elegans* larvae depleted of other dosage compensation proteins, but most of the larvae survive. We hypothesize that losing these mechanisms, including CEC-4 function, at the larval developmental stage does not result in outright lethality because cellular differentiation is more complete.

While DCC-mediated mechanisms are crucial for viability during the establishment of dosage compensation, our results demonstrate that they are not essential for survival during the maintenance stage. During larval and adult developmental stages, hermaphrodites survive without any known dosage compensation activity. This resilience raises questions about the necessity of continued X repression after embryonic development.

Acknowledgments

We thank Sarah VanDiepenbos, Hend Almunaidi, and Lillian Tushman for their contributions to a preliminary analysis of the *cec-4 and dpy-21* mutants, as well as all members of the laboratory for helpful discussions. We would like to thank the laboratory of Dr. JoAnne Engebrecht for sharing the JEL1197 strain [41].

Materials and Methods

Caenorhabditis elegans Strains

The strains used are shown in the table below. Strains were maintained at 20°C on nematode growth media (NGM) plates seeded with the *Escherichia coli* strain OP50 as a food source, as described in [67]. For some experiments requiring larger number of worms, strains were grown on high-growth media (HGM) plates were seeded with *E. coli* strain NA22, as described in [68].

Genotype	**Strain**	**Source**
Wild Type	Bristol N2	CGC
dpy-21(e428) V	EKM71	This study
cec-4 (ok3124) IV	EKM121	This study
cec-4 (ok3124) IV; *dpy-21(e428)* V	EKM222	This study
ieSi57[Peft-3::*TIR1*::mRuby::unc-54 3'UTR, cb-unc-119(+)] II; *dpy-27*::*AID::MYC* (xoe41) III	EKM237	This study
dpy-27::AID::MYC (xoe41) III	EKM227	[41]
dpy-27::AID::MYC (xoe41) III; *cec-4* (ok3124) IV	EKM233	This study
ieSi57[Peft-3::*TIR1*::mRuby*::unc-54* 3'UTR, *cb-unc-119*(+)] II; *dpy-27::AID::MYC*(xoe41) III; *cec-4*(ok3124) IV	EKM238	This study
wrdSi3 [*sun-1*p::*TIR1*::F2A::mTagBFP2::AID*::NLS::tbb-2 3'UTR] II; *dpy-27*(*xoe41*[*dpy-27::AID::myc*]) III; *him-8* (*me4*) IV	JEL1197	[41]
unc-119 (*ed3*); ieSi57 [*Peft-3*::*TIR1*::mRuby::*unc-54* 3'UTR, *cb-unc-119*(+)] II	CA1200	[42]

The alleles for *dpy-21 (e428)* and *cec-4 (ok3124)* were initially acquired from the *Caenorhabditis* Genetics Center (CGC) as the strains CB428 and RB2301, respectively. Each strain was backcrossed to Bristol N2 six times to generate the strains EKM71 *dpy-21 (e428)* and EKM121 *cec-4 (ok3124)*. EKM222 was obtained by crossing EKM71 to EKM121.

The strain JEL1197 was received from and generated by [41]. To isolate the *dpy-27::AID::MYC* (xoe41) allele, JEL1197 was crossed to wild type to produce EKM227. EKM227 was then crossed to CA1200 [42] to create EKM237.

To add *cec-4 (ok3124)* to the background, EKM227 was crossed with EKM121. The subsequent strain, EKM233, was crossed with CA1200 to generate EKM238.

736 **Antibodies**
737 Antibodies used in this study include rabbit anti-H4K20me1 (Abcam ab9051), rabbit
738 anti-DPY-27 [11], and goat anti-CAPG-1 [33]. Secondary antibodies for anti-goat and
739 anti-rabbit were purchased from Jackson Immunoresearch.

740 **Synchronized worm growth and collection**
741 To obtain synchronized worm populations, gravid adults were bleached to collect
742 embryos [69]. During bleaching, the hermaphrodites degrade and leave only embryos,
743 which are then collected. After washing with sterile 1X M9 salt solution [70], the
744 embryos are isolated and shaken slowly overnight in a flask containing M9 buffer to
745 allow them to hatch. Synchronized L1s were plated onto either NGM with OP-50 or
746 HGM with NA22 plates as needed. Synchronized L1s were used in RNA-seq, IF, and
747 larval development assays. After synchronization, L1s were grown to L3, or adult as
748 needed per assay.

749 **Auxin Treatment**
750 Strains were subjected to auxin (Thermo Fisher Alfa Aesar Indol-3-Acetic Acid
751 #A10556) by incorporation into NGM or HGM plates at a final concentration of 4mM, ,
752 as described in [42,71]. Auxin-containing plates were maintained in the dark at 4°C for
753 up to a month.

754 **Assay of viability upon auxin exposure initiated during**
755 **embryogenesis**
756 L4 hermaphrodites were placed on an auxin-containing plate to ensure all embryonic
757 development occurs while exposed to auxin. Plates were maintained in the dark at
758 20°C. Worms were placed on plates with or without auxin for an egg-laying period of 24
759 hours. After this period, the adult was removed from the plate, and the embryos laid
760 were counted. 24 hours later, the number of dead larvae and dead embryos were
761 quantified. Live adults were counted 3 days after the initial egg-laying period. Three
762 independent replicates were performed. Differences were evaluated using Fisher's
763 exact test comparing the numbers of dead and live progeny for each genotype.

764 **Assay of viability upon auxin exposure initiated during larval**
765 **development**
766 Experiments testing larval development began with synchronized L1 larvae. The
767 synchronized population was resuspended in M9 and split evenly between an auxin
768 plate and a plate without auxin for 3 days. Worms surviving after 3 days were counted.
769 Assuming an equal number of larvae initially plated, the final counts are reported as a
770 ratio of survival on auxin to survival off auxin. Three independent replicates were
771 performed. Differences were evaluated using Chi square test comparing the number of
772 surviving worms on auxin to the number surviving off auxin of each genotype.

773 **Brood Count Assay**

774 Young adult hermaphrodites were allowed to lay eggs on NGM and moved to new plate
775 each day until fertilized embryos were no longer produced. For each plate, after removal
776 of the parent, the number of embryos laid were counted, and after 24 hours, the number
777 of dead embryos were counted. After 3 days of development, the number of surviving
778 adults were counted. Embryonic viability was quantified as the number of hatched
779 embryos/total embryos. Larval viability was quantified as total number of adults/hatched
780 embryos.

781 **Immunofluorescence (IF)**

782 Hermaphrodite worms were dissected in 1x sperm salts (50 mM Pipes pH 7, 25 mM
783 KCl, 1 mM $MgSO_4$, 45 mM NaCl, and 2 mM $CaCl_2$) and fixed in 4% paraformaldehyde
784 (PFA) diluted in 1X sperm salts on a glass slide for 5 minutes in a humid chamber
785 containing PBS-T (PBS with 0.1% and Triton X-100). Slides were frozen on dry ice for
786 at least 20 minutes with a 20x20 mm coverslip over the diluted PFA and dissected *C.*
787 *elegans*. Using a razor blade, the coverslip was removed by flicking the coverslip off the
788 slide. The slides were then washed in PBS-T 3 times for 10 minutes each. 30µL of
789 diluted primary antibody was applied to each slide, a piece of parafilm was placed over
790 the spot with the antibody to slow evaporation. The slides were incubated in a humid
791 chamber at room temperature overnight. Slides were washed in PBS-T 3 times for 10
792 minutes and stained with corresponding secondary antibodies diluted 1:100 in PBS-T at
793 37°C for 1 hour. Three more washes in PBS-T were completed after the secondary
794 antibody incubation. In the third wash, the nucleus was stained using DAPI diluted in
795 PBS-T for 10 minutes at room temperature. Slides are mounted in Vectashield (Vector
796 Labs).

797 **Fluorescence *in situ* Hybridization (FISH)**

798 Degenerate Primer PCR was used to amplify purified yeast artificial chromosomes
799 (YACs) containing sequences corresponding to regions of the X chromosome and then
800 labeled with dCTP-Cy3 alongside standard nucleotides using random priming as in
801 [33,72]. The X paint FISH probe generated this way covers about 90% of the X. Adult
802 hermaphrodites were dissected on glass slides in 1x sperm salts and fixed in 4% PFA.
803 After 5 minutes of fixation, the specimen was covered with a 20x20 coverslip and placed
804 on dry ice for at least 20 minutes. The coverslip was then flicked off the slide with a
805 razor blade. Slides were washed in PBS-T three times and subjected to an ethanol
806 series of increasing concentrations (70%, 80%, 90%, 100% EtOH) for 2 minutes each,
807 after which the slides were air dried. To each slide, 10uL of X paint probe was added
808 and incubated at 37°C overnight. Next day, the slides were washed in a 39°C water
809 bath in 2x SSC/50% formamide three times, in 2X SSC solution three times for 5
810 minutes each, then in 1x SSC once for 10 minutes, followed by a room temperature
811 wash in 4x SSC. DAPI was included in the final 4x SSC wash and slides were mounted
812 using Vectashield. For FISH followed by IF, DAPI was excluded in the final 4X SSC
813 wash, after which IF was performed as described above.

Microscopy

Microscopy was performed using an Olympus BX61 microscope and a 60X APO oil immersion objective. Images were taken with a Hamamatsu ORCA-ER High-Resolution Monochrome Cooled CCD (IEEE 1394) camera. 3D images of nuclei were captured using 0.2-micrometer Z-spacing. The nuclei presented in this study are from intestinal cells. To observe signal depletion, exposure times were standardized to wild type.

Analysis of X Volume

Z-stacked images of intestinal nuclei of hermaphrodites were trimmed to 10-15 slices at 0.2 μM apart to include only planes with nuclear signal. Background signal was subtracted in ImageJ Fiji with a rolling ball radius of 50 pixels. After splitting the channels, the 3dManager from the 3dSuite plugin was used to create a three-dimensional ROI of the DAPI signal and a three-dimensional ROI of the FISH signal in the Cy3 channel [73]. The area of the Cy3 channel ROI inside the DAPI ROI was then compared in the 3dSuite 3DManager to find the X chromosome volume in the nucleus. The mask for the X chromosomes was limited to the area that overlaps with the DAPI mask signal, ensuring that the quantifications do not include non-specific staining of X paint FISH. The volume of the nucleus occupied is a ratio of the X signal relative to the DAPI signal measured in voxels (volumetric pixels).

Three-Zone Assay

From the images of nuclei stained using FISH targeting the X chromosome, the middle slice with the most in-focus FISH signal was selected. The background was subtracted in ImageJ FIJI with a rolling ball radius of 50 pixels. The DAPI and Cy3 channels were then split and thresholded. Using the native ROI manager in ImageJ FIJI, the threshold of the DAPI mask was used to draw three concentric ellipses that formed three zones of equal area in the nucleus. The Cy3 signal overlap with each zone was calculated using the ROI Manager to return the X chromosome FISH signal percentage in each zone. For this assay, only nuclei with smooth edges and an elliptical shape were used.

mRNA-seq

Synchronized L1s were placed on HGM plates with or without auxin and NA22 [74]. 24-hours later, L3 larvae were collected in M9. After pelleting, excess M9 was removed, and the remaining pellet was snap-frozen in liquid nitrogen with 1mL of Trizol. RNA was extracted and cleaned from the collected *C. elegans* using Qiagen RNeasy Kit. Reads were trimmed for quality use. Poly-A enrichment, library prep, and next-generation sequencing were conducted in the Advanced Genomics Core at the University of Michigan. RNA was assessed for quality using the TapeStation or Bioanalyzer (Agilent). Samples with RINs (RNA Integrity Numbers) of 8 or greater were subjected to Poly-A enrichment using the NEBNext Poly(A) mRNA Magnetic Isolation Module (NEB catalog number E7490). NEBNext Ultra II Directional RNA Library Prep Kit for Illumina (catalog number E7760L) and NEBNext Multiplex Oligos for Illumina Unique dual (catalog number E6448S) were then used for library prep. The mRNA was fragmented and

copied into first-strand cDNA using reverse transcriptase and random primers. The 3' ends of the cDNA were then adenylated, and adapters were ligated. The PCR products were purified and enriched to create the final cDNA library. Qubit hsDNA (Thermofisher) and LabChip (Perkin Elmer) checked the final libraries for quality and quantity. The samples were pooled and sequenced on the Illumina NovaSeqX 10B paired-end 150bp, according to the manufacturer's recommended protocols. BCL Convert Conversion Software v4.0 (Illumina) generated de-multiplexed Fastq files. The reads were trimmed using CutAdapt v2.3. FastQC v0.11.8 was used to ensure the quality of data [75,76]. Reads were mapped to the reference genome WBcel235 and read counts were generated using Salmon v1.9.0 [77]. Differential gene expression analysis was performed using DESeq2 v1.42.0 [78]. Downstream analyses were performed using R scripts and packages.

References

1. Ohno S. Sex Chromosomes and Sex-Linked Genes: Springer Berlin Heidelberg; 1967. doi:10.1007/978-3-642-88178-7

2. Lau AC, Csankovszki G. Balancing up and downregulation of the C. elegans X chromosomes. Curr Opin Genet Dev. 2015;31: 50–56. doi:10.1016/j.gde.2015.04.001

3. Madl JE, Herman RK. Polyploids and sex determination in Caenorhabditis elegans. Genetics. 1979;93: 393–402.

4. Nusbaum C, Meyer BJ. The Caenorhabditis Elegans Gene Sdc-2 Controls Sex Determination and Dosage Compensation in Xx Animals. Genetics. 1989;122: 579–593.

5. Hodgkin J. X chromosome dosage and gene expression in Caenorhabditis elegans: Two unusual dumpy genes. Mol Gen Genet. 1983;192: 452–458. doi:10.1007/BF00392190

6. Meyer BJ, Casson LP. Caenorhabditis elegans compensates for the difference in X chromosome dosage between the sexes by regulating transcript levels. Cell. 1986;47: 871–881. doi:10.1016/0092-8674(86)90802-0

7. Hirano T. Condensins: organizing and segregating the genome. Curr Biol CB. 2005;15: R265-275. doi:10.1016/j.cub.2005.03.037

8. Ganji M, Shaltiel IA, Bisht S, Kim E, Kalichava A, Haering CH, et al. Real-time imaging of DNA loop extrusion by condensin. Science. 2018;360: 102–105. doi:10.1126/science.aar7831

9. Kong M, Cutts EE, Pan D, Beuron F, Kaliyappan T, Xue C, et al. Human Condensin I and II Drive Extensive ATP-Dependent Compaction of Nucleosome-Bound DNA. Mol Cell. 2020;79: 99-114.e9. doi:10.1016/j.molcel.2020.04.026

892 10. Hirano T. Condensins: universal organizers of chromosomes with diverse
893 functions. Genes Dev. 2012;26: 1659–1678. doi:10.1101/gad.194746.112

894 11. Csankovszki G, Collette K, Spahl K, Carey J, Snyder M, Petty E, et al. Three
895 distinct condensin complexes control C. elegans chromosome dynamics. Curr Biol.
896 2009;19: 9–19. doi:10.1016/j.cub.2008.12.006

897 12. Mets DG, Meyer BJ. Condensins Regulate Meiotic DNA Break Distribution, thus
898 Crossover Frequency, by Controlling Chromosome Structure. Cell. 2009;139: 73–
899 86. doi:10.1016/j.cell.2009.07.035

900 13. Hirano T, Kobayashi R, Hirano M. Condensins, chromosome condensation protein
901 complexes containing XCAP-C, XCAP-E and a Xenopus homolog of the
902 Drosophila Barren protein. Cell. 1997;89: 511–521. doi:10.1016/s0092-
903 8674(00)80233-0

904 14. Paul MR, Hochwagen A, Ercan S. Condensin action and compaction. Curr Genet.
905 2019;65: 407–415. doi:10.1007/s00294-018-0899-4

906 15. Chuang PT, Albertson DG, Meyer BJ. DPY-27:a chromosome condensation
907 protein homolog that regulates C. elegans dosage compensation through
908 association with the X chromosome. Cell. 1994;79: 459–474. doi:10.1016/0092-
909 8674(94)90255-0

910 16. Hagstrom KA, Holmes VF, Cozzarelli NR, Meyer BJ. C. elegans condensin
911 promotes mitotic chromosome architecture, centromere organization, and sister
912 chromatid segregation during mitosis and meiosis. Genes Dev. 2002;16: 729–742.
913 doi:10.1101/gad.968302

914 17. Lau AC, Nabeshima K, Csankovszki G. The C. elegans dosage compensation
915 complex mediates interphase X chromosome compaction. Epigenetics Chromatin.
916 2014;7: 31. doi:10.1186/1756-8935-7-31

917 18. Lau AC, Csankovszki G. Condensin-mediated chromosome organization and gene
918 regulation. Front Genet. 2014;5: 473. doi:10.3389/fgene.2014.00473

919 19. Crane E, Bian Q, McCord RP, Lajoie BR, Wheeler BS, Ralston EJ, et al.
920 Condensin-driven remodelling of X chromosome topology during dosage
921 compensation. Nature. 2015;523: 240–244. doi:10.1038/nature14450

922 20. Kim J, Jimenez DS, Ragipani B, Zhang B, Street LA, Kramer M, et al. Condensin
923 DC loads and spreads from recruitment sites to create loop-anchored TADs in C.
924 elegans. Tyler JK, editor. eLife. 2022;11: e68745. doi:10.7554/eLife.68745

925 21. Chu DS, Dawes HE, Lieb JD, Chan RC, Kuo AF, Meyer BJ. A molecular link
926 between gene-specific and chromosome-wide transcriptional repression. Genes
927 Dev. 2002;16: 796–805. doi:10.1101/gad.972702

928 22. Yonker SA, Meyer BJ. Recruitment of C. elegans dosage compensation proteins
929 for gene-specific versus chromosome-wide repression. Development. 2003;130:
930 6519–6532. doi:10.1242/dev.00886

931 23. Pferdehirt RR, Meyer BJ. SUMOylation is essential for sex-specific assembly and
932 function of the Caenorhabditis elegans dosage compensation complex on X
933 chromosomes. Proc Natl Acad Sci. 2013;110: E3810–E3819.
934 doi:10.1073/pnas.1315793110

935 24. Kruesi WS, Core LJ, Waters CT, Lis JT, Meyer BJ. Condensin controls recruitment
936 of RNA polymerase II to achieve nematode X-chromosome dosage compensation.
937 Elife. 2013;2: e00808. doi:10.7554/eLife.00808

938 25. Brejc K, Bian Q, Uzawa S, Wheeler BS, Anderson EC, King DS, et al. Dynamic
939 Control of X Chromosome Conformation and Repression by a Histone H4K20
940 Demethylase. Cell. 2017;171: 85-102.e23. doi:10.1016/j.cell.2017.07.041

941 26. Wells MB, Snyder MJ, Custer LM, Csankovszki G. Caenorhabditis elegans dosage
942 compensation regulates histone H4 chromatin state on X chromosomes. Mol Cell
943 Biol. 2012;32: 1710–1719. doi:10.1128/MCB.06546-11

944 27. Vielle A, Lang J, Dong Y, Ercan S, Kotwaliwale C, Rechtsteiner A, et al.
945 H4K20me1 contributes to downregulation of X-linked genes for C. elegans dosage
946 compensation. PLoS Genet. 2012;8: e1002933. doi:10.1371/journal.pgen.1002933

947 28. Breimann L, Morao AK, Kim J, Sebastian Jimenez D, Maryn N, Bikkasani K, et al.
948 The histone H4 lysine 20 demethylase DPY-21 regulates the dynamics of
949 condensin DC binding. J Cell Sci. 2022;135: jcs258818. doi:10.1242/jcs.258818

950 29. Kramer M, Kranz A-L, Su A, Winterkorn LH, Albritton SE, Ercan S. Developmental
951 Dynamics of X-Chromosome Dosage Compensation by the DCC and H4K20me1
952 in C. elegans. PLoS Genet. 2015;11: e1005698. doi:10.1371/journal.pgen.1005698

953 30. Towbin BD, González-Aguilera C, Sack R, Gaidatzis D, Kalck V, Meister P, et al.
954 Step-wise methylation of histone H3K9 positions heterochromatin at the nuclear
955 periphery. Cell. 2012;150: 934–947. doi:10.1016/j.cell.2012.06.051

956 31. Ikegami K, Egelhofer TA, Strome S, Lieb JD. Caenorhabditis elegans chromosome
957 arms are anchored to the nuclear membrane via discontinuous association with
958 LEM-2. Genome Biol. 2010;11: R120. doi:10.1186/gb-2010-11-12-r120

959 32. Gonzalez-Sandoval A, Towbin BD, Kalck V, Cabianca DS, Gaidatzis D, Hauer MH,
960 et al. Perinuclear Anchoring of H3K9-Methylated Chromatin Stabilizes Induced Cell
961 Fate in C. elegans Embryos. Cell. 2015;163: 1333–1347.
962 doi:10.1016/j.cell.2015.10.066

963 33. Snyder MJ, Lau AC, Brouhard EA, Davis MB, Jiang J, Sifuentes MH, et al.
964 Anchoring of Heterochromatin to the Nuclear Lamina Reinforces Dosage

965 Compensation-Mediated Gene Repression. PLoS Genet. 2016;12: e1006341.
966 doi:10.1371/journal.pgen.1006341

967 34. Dawes HE, Berlin DS, Lapidus DM, Nusbaum C, Davis TL, Meyer BJ. Dosage
968 compensation proteins targeted to X chromosomes by a determinant of
969 hermaphrodite fate. Science. 1999;284: 1800–1804.

970 35. Meyer BJ. Targeting X chromosomes for repression. Curr Opin Genet Dev.
971 2010;20: 179–189. doi:10.1016/j.gde.2010.03.008

972 36. Custer LM, Snyder MJ, Flegel K, Csankovszki G. The onset of C. elegans dosage
973 compensation is linked to the loss of developmental plasticity. Dev Biol. 2014;385:
974 279–290. doi:10.1016/j.ydbio.2013.11.001

975 37. Yuzyuk T, Fakhouri THI, Kiefer J, Mango SE. The polycomb complex protein mes-
976 2/E(z) promotes the transition from developmental plasticity to differentiation in C.
977 elegans embryos. Dev Cell. 2009;16: 699–710. doi:10.1016/j.devcel.2009.03.008

978 38. Sulston JE, Schierenberg E, White JG, Thomson JN. The embryonic cell lineage of
979 the nematode Caenorhabditis elegans. Dev Biol. 1983;100: 64–119.
980 doi:10.1016/0012-1606(83)90201-4

981 39. Plenefisch JD, DeLong L, Meyer BJ. Genes that implement the hermaphrodite
982 mode of dosage compensation in Caenorhabditis elegans. Genetics. 1989;121:
983 57–76. doi:10.1093/genetics/121.1.57

984 40. Cabianca DS, Muñoz-Jiménez C, Kalck V, Gaidatzis D, Padeken J, Seeber A, et
985 al. Active chromatin marks drive spatial sequestration of heterochromatin in C.
986 elegans nuclei. Nature. 2019;569: 734–739. doi:10.1038/s41586-019-1243-y

987 41. Li Q, Kaur A, Mallory B, Hariri S, Engebrecht J. Inducible degradation of dosage
988 compensation protein DPY-27 facilitates isolation of *Caenorhabditis elegans* males
989 for molecular and biochemical analyses. Ward J, editor. G3
990 GenesGenomesGenetics. 2022;12: jkac085. doi:10.1093/g3journal/jkac085

991 42. Zhang L, Ward JD, Cheng Z, Dernburg AF. The auxin-inducible degradation (AID)
992 system enables versatile conditional protein depletion in C. elegans. Development.
993 2015;142: 4374–4384. doi:10.1242/dev.129635

994 43. Hedgecock EM, White JG. Polyploid tissues in the nematode *Caenorhabditis*
995 *elegans*. Dev Biol. 1985;107: 128–133. doi:10.1016/0012-1606(85)90381-1

996 44. Kelly WG, Schaner CE, Dernburg AF, Lee M-H, Kim SK, Villeneuve AM, et al. X-
997 chromosome silencing in the germline of C. elegans. Dev Camb Engl. 2002;129:
998 479–492.

45. Crittenden SL, Leonhard KA, Byrd DT, Kimble J. Cellular Analyses of the Mitotic Region in the Caenorhabditis elegans Adult Germ Line. Mol Biol Cell. 2006;17: 3051–3061. doi:10.1091/mbc.E06-03-0170

46. Schiksnis EC, Nicholson AL, Modena MS, Pule MN, Arribere JA, Pasquinelli AE. Auxin-independent depletion of degron-tagged proteins by TIR1. MicroPublication Biol. 2020: 10.17912/micropub.biology.000213. doi:10.17912/micropub.biology.000213

47. Natsume T, Kiyomitsu T, Saga Y, Kanemaki MT. Rapid Protein Depletion in Human Cells by Auxin-Inducible Degron Tagging with Short Homology Donors. Cell Rep. 2016;15: 210–218. doi:10.1016/j.celrep.2016.03.001

48. Martinez MA, Kinney BA, Medwig-Kinney TN, Ashley G, Ragle JM, Johnson L, et al. Rapid degradation of Caenorhabditis elegans proteins at single-cell resolution with a synthetic auxin. G3 Genes Genomes Genet. 2020;10: 267–280.

49. Samejima K, Booth DG, Ogawa H, Paulson JR, Xie L, Watson CA, et al. Functional analysis after rapid degradation of condensins and 3D-EM reveals chromatin volume is uncoupled from chromosome architecture in mitosis. J Cell Sci. 2018;131: jcs210187. doi:10.1242/jcs.210187

50. Hirano T, Mitchison TJ. A heterodimeric coiled-coil protein required for mitotic chromosome condensation in vitro. Cell. 1994;79: 449–458. doi:10.1016/0092-8674(94)90254-2

51. Houlard M, Godwin J, Metson J, Lee J, Hirano T, Nasmyth K. Condensin confers the longitudinal rigidity of chromosomes. Nat Cell Biol. 2015;17: 771–781. doi:10.1038/ncb3167

52. Piskadlo E, Tavares A, Oliveira RA. Metaphase chromosome structure is dynamically maintained by condensin I-directed DNA (de)catenation. eLife. 2017;6: e26120. doi:10.7554/eLife.26120

53. Zhiteneva A, Bonfiglio JJ, Makarov A, Colby T, Vagnarelli P, Schirmer EC, et al. Mitotic post-translational modifications of histones promote chromatin compaction in vitro. Open Biol. 2017;7: 170076. doi:10.1098/rsob.170076

54. Corvalan AZ, Coller HA. Methylation of histone 4's lysine 20: a critical analysis of the state of the field. Physiol Genomics. 2021;53: 22–32. doi:10.1152/physiolgenomics.00128.2020

55. Wilkins BJ, Rall NA, Ostwal Y, Kruitwagen T, Hiragami-Hamada K, Winkler M, et al. A cascade of histone modifications induces chromatin condensation in mitosis. Science. 2014;343: 77–80. doi:10.1126/science.1244508

56. Javasky E, Shamir I, Gandhi S, Egri S, Sandler O, Rothbart SB, et al. Study of mitotic chromatin supports a model of bookmarking by histone modifications and

1036 reveals nucleosome deposition patterns. Genome Res. 2018;28: 1455–1466.
1037 doi:10.1101/gr.230300.117

1038 57. Methot SP, Padeken J, Brancati G, Zeller P, Delaney CE, Gaidatzis D, et al.
1039 H3K9me selectively blocks transcription factor activity and ensures differentiated
1040 tissue integrity. Nat Cell Biol. 2021;23: 1163–1175. doi:10.1038/s41556-021-
1041 00776-w

1042 58. Anderson EC, Frankino PA, Higuchi-Sanabria R, Yang Q, Bian Q, Podshivalova K,
1043 et al. X Chromosome Domain Architecture Regulates Caenorhabditis elegans
1044 Lifespan but Not Dosage Compensation. Dev Cell. 2019;51: 192-207.e6.
1045 doi:10.1016/j.devcel.2019.08.004

1046 59. Csankovszki G, Panning B, Bates B, Pehrson JR, Jaenisch R. Conditional deletion
1047 of Xist disrupts histone macroH2A localization but not maintenance of X
1048 inactivation. Nat Genet. 1999;22: 323–324. doi:10.1038/11887

1049 60. Csankovszki G, Nagy A, Jaenisch R. Synergism of Xist RNA, DNA methylation,
1050 and histone hypoacetylation in maintaining X chromosome inactivation. J Cell Biol.
1051 2001;153: 773–783. doi:10.1083/jcb.153.4.773

1052 61. Heard E, Disteche CM. Dosage compensation in mammals: fine-tuning the
1053 expression of the X chromosome. Genes Dev. 2006;20: 1848–1867.
1054 doi:10.1101/gad.1422906

1055 62. Leonhardt H, Page AW, Weier HU, Bestor TH. A targeting sequence directs DNA
1056 methyltransferase to sites of DNA replication in mammalian nuclei. Cell. 1992;71:
1057 865–873. doi:10.1016/0092-8674(92)90561-p

1058 63. Audergon PNCB, Catania S, Kagansky A, Tong P, Shukla M, Pidoux AL, et al.
1059 Epigenetics. Restricted epigenetic inheritance of H3K9 methylation. Science.
1060 2015;348: 132–135. doi:10.1126/science.1260638

1061 64. Margueron R, Justin N, Ohno K, Sharpe ML, Son J, Drury III WJ, et al. Role of the
1062 polycomb protein EED in the propagation of repressive histone marks. Nature.
1063 2009;461: 762–767. doi:10.1038/nature08398

1064 65. Hansen KH, Bracken AP, Pasini D, Dietrich N, Gehani SS, Monrad A, et al. A
1065 model for transmission of the H3K27me3 epigenetic mark. Nat Cell Biol. 2008;10:
1066 1291–1300. doi:10.1038/ncb1787

1067 66. Liu W, Tanasa B, Tyurina OV, Zhou TY, Gassmann R, Liu WT, et al. PHF8
1068 mediates histone H4 lysine 20 demethylation events involved in cell cycle
1069 progression. Nature. 2010;466: 508–512. doi:10.1038/nature09272

1070 67. Brenner S. The genetics of Caenorhabditis elegans. Genetics. 1974;77: 71–94.

68. Zhang S. Cell isolation and culture. WormBook. 2013; 1–39. doi:10.1895/wormbook.1.157.1

69. Porta-de-la-Riva M, Fontrodona L, Villanueva A, Cerón J. Basic Caenorhabditis elegans Methods: Synchronization and Observation. J Vis Exp JoVE. 2012; 4019. doi:10.3791/4019

70. M9 Buffer for Worms. Cold Spring Harb Protoc. 2014;2014: pdb.rec081315. doi:10.1101/pdb.rec081315

71. Ashley GE, Duong T, Levenson MT, Martinez MAQ, Johnson LC, Hibshman JD, et al. An expanded auxin-inducible degron toolkit for *Caenorhabditis elegans*. Greenstein D, editor. Genetics. 2021;217: iyab006. doi:10.1093/genetics/iyab006

72. Nabeshima K, Mlynarczyk-Evans S, Villeneuve AM. Chromosome Painting Reveals Asynaptic Full Alignment of Homologs and HIM-8–Dependent Remodeling of X Chromosome Territories during Caenorhabditis elegans Meiosis. PLoS Genet. 2011;7: e1002231. doi:10.1371/journal.pgen.1002231

73. Ollion J, Cochennec J, Loll F, Escudé C, Boudier T. TANGO: a generic tool for high-throughput 3D image analysis for studying nuclear organization. Bioinforma Oxf Engl. 2013;29: 1840–1841. doi:10.1093/bioinformatics/btt276

74. Zhang S, Kuhn JR. Cell isolation and culture. WormBook: The Online Review of C elegans Biology [Internet]. WormBook; 2018. Available: https://www.ncbi.nlm.nih.gov/books/NBK153594/

75. Martin M. Cutadapt removes adapter sequences from high-throughput sequencing reads. EMBnet.journal. 2011;17: 10–12. doi:10.14806/ej.17.1.200

76. FastQC. 2015. Available: https://qubeshub.org/resources/fastqc

77. Patro R, Duggal G, Love MI, Irizarry RA, Kingsford C. Salmon provides fast and bias-aware quantification of transcript expression. Nat Methods. 2017;14: 417–419. doi:10.1038/nmeth.4197

78. Love MI, Huber W, Anders S. Moderated estimation of fold change and dispersion for RNA-seq data with DESeq2. Genome Biol. 2014;15: 550. doi:10.1186/s13059-014-0550-8

Supporting information

S1 Fig. Comparison of all rings from the three-zone assay of X localization within the nucleus with and without auxin treatment. (**A)** Three-zone assay for the X paint FISH signal (n = 20 nuclei) in strains grown without auxin showing all three concentric zones. **(B)** Three-zone assay for the X paint FISH signal (n = 20 nuclei) in strains grown in the presence of auxin.

1107 **S2 Fig. mRNA-seq analysis of *dpy-27::AID* strains. (A-D)** Boxplots depicting the
1108 distribution of the expression difference of X-linked genes and expression difference of
1109 genes on autosomes. Gene expression is plotted as the log2 ratio of the strains being
1110 compared. Statistical significance is determined by the differences in gene expression
1111 between the X and autosomes by a Wilcoxon rank-sum test. (n.s. = not significant, * = p
1112 < 0.05, ** = p<0.01, *** = p < 0.001) **(E)** Principal component analysis (PCA) plot
1113 depicting the relationships among *TIR1; dpy-27::AID*, and *TIR1; dpy-27::AID; cec-4*.
1114 Auxin treatment is indicated alongside the corresponding genotype in the figure.

1115 **S3 Fig. RNA seq analysis of *cec-4* and *dpy-*21 mutants.** Principal component
1116 analysis (PCA) plot depicting the relationships among wild-type, single mutants (*cec-4*
1117 and *dpy-21*), and double mutants (*cec-4; dpy-21*) based on gene expression profiles.

1118 **S1 File. Statistical analysis of the survival of embryo in the presence or absence**
1119 **of auxin.**

1120 **S2 File. Statistical analysis of the survival of larvae in the presence or absence of**
1121 **auxin.**

1122 **S3 File. Statistical analysis of X chromosome decondensation.**

1123 **S4 File. Statistical analysis of X chromosome localization within the nucleus via**
1124 **the three-zone assay.**

1125 **S5 File. Statistical analysis of mRNA-seq.**

1126 **S6 File. Statistical analysis of the broods laid by worms containing *cec-4* and *dpy-***
1127 ***21* mutations.**

1128 **S7 File. Statistical analysis of the decondensation of the X chromosome in *cec-4***
1129 **and *dpy-21* containing mutants.**

1130